Salinity frontogenesis/frontolysis in the northeastern subtropical Pacific region

Shun Ohishi[1*], Shota Katsura[2], and Hidenori Aiki[1]

[1] Institute for Space-Earth Environmental Research, Nagoya University, Nagoya, Japan

[2] Scripps Institution of Oceanography, University of California, San Diego, La Jolla

Climate Dynamics (Revised)

Jul. 3 2019

*Corresponding author address: Dr. Shun Ohishi, Institute for Space-Earth Environmental Research, Nagoya University, Furo-cho, Chikusa-ku, Nagoya, Aichi, 464-8601, Japan. E-mail: ohishi@isee.nagoya-u.ac.jp, TEL: +81-52-789-3434, FAX: +81-52-788-6206

Abstract (250/150–250 words)

Detailed mechanisms of reinforcement/relaxation of a sea surface salinity front, i.e. frontogenesis/frontolysis, in the northeastern subtropical Pacific region are investigated using observational datasets. Throughout the year, meridional shears of zonal wind induce meridional ageostrophic convergence around the front. Saltier water is advected on the southern side than the northern side, and thus the convergence contributes to frontogenesis. The evaporation and precipitation gradients also strengthen the front, because higher sea surface temperatures on the southern side induce stronger evaporation through the formation of higher surface saturated specific humidity, and because the precipitation rate is low in the southern region in association with the subtropical high of the atmosphere. However, in summer–autumn when the mixed layer is seasonally thin and evaporation exceeds precipitation, the frontogenesis by the freshwater flux gradient is damped by the mixed layer depth (MLD) gradient. This is attributed to the thicker mixed layer south of the front being less sensitive to freshwater fluxes. During the mixed-layer deepening phase, the mixed layer on the southern side entrains lower salinity water from the lower layer, and thus the entrainment relaxes the front. Therefore, it is shown that the gradients of ageostrophic advection, evaporation, and precipitation result in frontogenesis, while those of MLD and entrainment cause frontolysis. Furthermore, a metric that quantifies the relative importance of the horizontal gradients of freshwater fluxes and MLD for salinity frontogenesis/frontolysis is proposed. Over the large domain, contribution from the horizontal gradient of freshwater fluxes dominates over that of MLD.

Keywords(4/4–6 Keywords)

Sea surface salinity front, frontogenesis/frontolysis, the northeastern subtropical Pacific, freshwater flux frontogenesis metric

1. Introduction

Salinity is an important variable for ocean circulation because of its influences on the density distribution of sea water, and for climate because it modifies ocean sensitivity to air-sea heat and momentum exchange changing density stratification (e.g. Vialard and Delecluse 1998a, b). Before 1990s salinity observation had been limited to only ships and mooring buoys, and thus understanding of salinity spatiotemporal variations through mixed-layer salinity (MLS) budget analysis was confined to particular areas such as the tropical Pacific and Atlantic regions (Cronin and McPhaden 1998; Foltz et al. 2004), where the Tropical Atmosphere Ocean/Triangle Trans-Ocean buoy Network (TAO/TRITON; McPhaden 1995; Ando and Kuroda 2002) and Prediction and Research Moored Array in the Atlantic (PIRATA; Bourlès et al. 2008) buoys are deployed and intensive observations called as Tropical Ocean Global Atmosphere Coupled Ocean-Atmosphere Response Experiment (TOGA-COARE; Webster and Lukas 1992) were carried out. The global salinity observations by Argo profiling floats since 2000s (Roemmich et al. 2009) and satellites since 2010 (Mecklenburg et al. 2012) have brought drastic changes to enable us to more accurately capture the salinity horizontal and vertical structure.

At present, sea surface salinity (SSS) fronts can be detected in many parts of the global ocean (Kao and Lagerloef 2015; Yu 2015). While both SSS and SST fronts are distributed in western boundary currents and their extension regions throughout the year, SSS fronts alone exist in eastern subtropical Pacific and equatorial regions, and off the Amazon river (Fig. 1). Katsura (2018) proposed that SSS fronts in the eastern subtropical Pacific have the relationship with the formation

of eastern subtropical mode water (ESTMW; e.g. Hautala and Roemmich 1998), which acts as a reservoir of physical and biogeochemical properties, through maintenance of weak vertical density stratification. Cronin and McPhaden (2002) and Katsura et al. (2015) demonstrated importance of SSS fronts that their vertical tilting causes salinity stratification leading to the barrier layer. Therefore, SSS fronts play important roles in the formation of the mode water and barrier layer.

Detailed reinforcement/relaxation processes of SSS fronts, i.e. SSS frontogenesis/frontolysis, have yet to be investigated, while recent studies reported detailed mechanisms of SST frontogenesis/frontolysis in the Agulhas Return Current (ARC; Tozuka and Cronin 2014; Ohishi et al. 2016, 2017) and Kuroshio Extension (KE; Tozuka et al. 2017) regions, and Japan Sea (JS; Ohishi et al. 2019). They revealed that the mixed layer depth (MLD) gradient have substantial impacts on frontogenesis/frontolysis by surface heat fluxes (In this paper, the gradient indicates the meridional gradient, unless otherwise specified). In the ARC region and JS, frontolysis results from weaker heating in summer and stronger cooling in winter caused by the stronger turbulent heat release on the warmer side of the front than the cooler side (Tozuka and Cronin 2014; Ohishi et al. 2016; Ohishi et al. 2019). In addition, the MLD gradient enhances and damps the frontolysis by the surface net heat fluxes (NHF) gradient in summer and winter, respectively, because the thicker mixed layer on the warmer side is less sensitive to net heating in summer and cooling in winter. In contrast, surface heat fluxes contribute to frontogenesis in the wintertime KE region, because frontogenesis caused by the MLD gradient exceeds weak frontolysis by the small cooling difference (Konda et al. 2010; Tozuka et al. 2017). Tozuka et al. (2018) proposed a metric to quantify the relative importance of

99 the horizontal NHF and MLD gradients for reinforcement/relaxation processes of
100 the horizontal gradient of mixed layer temperatures (MLTs), and revealed that their
101 roles are geographically and temporally variable.

102 Since the MLS budget equation has a similar form to the MLT, detailed
103 processes of SSS frontogenesis/frontolysis could be investigated applying the
104 method used for SST frontogenesis/frontolysis. In this study, we focus on an SSS
105 front in the northeastern subtropical Pacific region (Fig. 1b), because there are
106 single and strong SSS front and the horizontal gradient of SSS forms that of sea
107 surface density (SSD) (see Appendix 1). The objectives of this study are to
108 quantitatively investigate salinity frontogenesis/frontolysis in the northeastern
109 subtropical Pacific region using observational datasets. For extending results
110 obtained in the northeastern subtropical Pacific to the global ocean, we propose a
111 metric to quantify the relative contributions of the horizontal gradients of
112 freshwater fluxes and MLD. This paper is organized as follow. Observational datasets
113 and methodology used in this study are provided in the next section. Section 3
114 describes characteristics of the SSS front and the detail of salinity
115 frontogenesis/frontolysis in the northeastern subtropical Pacific region. In Section
116 4, the metric is introduced and applied to the global ocean. Conclusions are given in
117 the final section.
118

119 **2. Data and methodology**

120 **2.1 Data**

121 Monthly temperature and salinity climatology is obtained from the Monthly
122 Isopycnal/Mixed-layer Ocean Climatology (MIMOC; Schmidtko et al. 2013) on 0.5°

123 longitude × 0.5° latitude grid with 81 layers. MIMOC is established using mainly the
124 Argo float profiles in 2007–2011 and suitable for frontal studies because of applying
125 weighting and covariance functions to maintain the sharpness of fronts. In this study,
126 MLD is defined as a depth at which potential density is greater by 0.125 kg m^{-3} than
127 the density at the sea surface and detected using a spline function of Akima (1970)
128 at 0.1 m interval. Mixed layer salinity (MLS) is vertical-averaged salinity within a
129 mixed layer and estimated from the integrated spline function of Akima (1970). We
130 use zonal/meridional wind stress, latent heat fluxes, wind speed, and air and surface
131 saturated specific humidity from the Japanese Ocean Flux Data Sets with Use of
132 Remote-Sensing Observations 3 (J-OFURO 3; Tomita et al. 2019) with a horizontal
133 resolution of 0.25°. Precipitation is obtained from the Tropical Rainfall Measuring
134 Mission (TRMM) 3B43 version 7
135 (http://apdrc.soest.hawaii.edu/datadoc/trmm_3b43.php) with a horizontal
136 resolution of 0.25°. We adopt sea level pressure (SLP) from the Japanese 55-year
137 Reanalysis (JRA55; Kobayashi et al. 2015) on 1.25° longitude × 1.25° latitude grid.
138 Sea surface height (SSH) is derived from Archiving, Validation and Interpretation of
139 Satellite Oceanographic data (AVISO; Ducet et al. 2000) with a horizontal resolution
140 of 0.25°. In this study, we use monthly climatology of the above datasets averaged in
141 2007–2011 corresponding to the MIMOC.
142
143 **2.2 Methodology**
144 To quantitatively investigate salinity frontogenesis/frontolysis, we take the
145 meridional derivative of the MLS S_{mix} budget equation (e.g. Cronin and McPhaden
146 1998; Foltz et al. 2004) to yield the frontogenesis rate equation (c.f. Ohishi et al. 2016,

2017):

$$\frac{\partial}{\partial t}\left(\frac{\partial S_{mix}}{\partial y}\right) = -\frac{\partial}{\partial y}(\boldsymbol{u_{mix}} \cdot \boldsymbol{\nabla} S_{mix}) + \frac{\partial}{\partial y}\left(\frac{(E-P)S_{mix}}{H}\right) - \frac{\partial}{\partial y}\left(\frac{\Delta S}{H} w_e\right) + (res), \quad (1)$$

where $\boldsymbol{u_{mix}}$ is horizontal velocity within the mixed layer that may be separated into geostrophic $\boldsymbol{u^g_{mix}}$ and ageostrophic $\boldsymbol{u^a_{mix}}$ components. Geostrophic vertical shears may not be so large around the SSS front in the northeastern subtropical Pacific region because of the small horizontal SST gradient magnitude (Fig. 1), and thus $\boldsymbol{u^a_{mix}}$ can be estimated based on the classical Ekman theory (Ekman 1905; Cronin and Tozuka 2016):

$$\boldsymbol{u^a_{mix}} = \frac{\boldsymbol{U^a}}{H} = -\frac{\boldsymbol{k} \times \boldsymbol{\tau}}{\rho_0 f H}, \quad (2)$$

where $\boldsymbol{U^a}$ is the Ekman transport, H is MLD, $\boldsymbol{k}$ is the unit vector in the vertical direction, $\boldsymbol{\tau}$ is the horizontal wind stress vector, ρ_0 $(= 1026\ kg\ m^{-3})$ is the reference density of sea water, and f is the Coriolis parameter at a given latitude. We have assumed that the Ekman layers correspond to mixed layers. The symbol E in Eq. (1) is the rate of evaporation and calculated from latent heat fluxes Q_{lh} according to $E = Q_{lh}/\rho_f L$, where ρ_f $(= 1000\ kg\ m^{-3})$ is the density of freshwater and L $(\approx 2.5 \times 10^3\ J\ g^{-1})$ is the latent heat of evaporation. The symbol P in Eq. (1) is the rate of precipitation, and ΔS is the salinity difference between the mixed and entrained layer. In this study, salinity 20m below the base of the mixed layer

167 S_{-H-20m} is adopted for the entrained salinity (c.f. Ren and Riser 2009; Katsura et al.
168 2013). w_e is the entrainment velocity, and assumed to be the MLD tendency during
169 mixed-layer deepening phases on both sides of the front and otherwise vanish in this
170 study (e.g. Niiler and Kraus 1977). (res) includes the sheared stratified
171 convergence term, contributions from horizontal induction and vertical velocity,
172 horizontal/vertical diffusion term, and temporal and spatial covariance terms. The
173 frontogenesis rate equation [Eq. (1)] shows that the tendency of MLS fronts is
174 expressed as the sum of contributions from horizontal advection, freshwater fluxes,
175 entrainment gradient, and the residual.
176
177 **3. Salinity frontogenesis/frontolysis in the northeastern subtropical Pacific**
178 **region**
179 **3.1 Salinity frontogenesis/frontolysis**
180 To examine characteristics of the SSS front in the northeastern subtropical
181 Pacific region, its intensity and meridional position are defined as a maximum of the
182 horizontal SSS gradient magnitude in 25°–40°N and its latitude at each longitude,
183 respectively. Figure 2 shows their mean and standard deviations estimated from
184 monthly climatologies. Single SSS front is located in 30°–35°N, and in 150°–140°W
185 it has strong intensity of 0.3–0.4 $(100\text{km})^{-1}$ and stable meridional position. This SSS
186 front undergoes a seasonality of stronger intensity in summer than winter (Fig. 3).
187 To quantitatively investigate the frontogenesis/frontolysis, we estimate
188 each term of the frontogenesis rate equation [Eq. (1)]. Here, contributions from
189 geostrophic advection substitute to the residual term [the last term on the right-
190 hand side (RHS) of Eq. (1)], because spatially irregular pattern of geostrophic

velocity with various directions can be detected on either sides of the SSS front in the northeastern subtropical Pacific region and the estimate might include uncertainties (figure not shown). Thus, the frontogenesis rate equation [Eq. (1)] is modified as

$$\frac{\partial}{\partial t}\left(\frac{\partial S_{mix}}{\partial y}\right) = -\frac{\partial}{\partial y}(\boldsymbol{u}^{\boldsymbol{a}}_{\boldsymbol{mix}} \cdot \boldsymbol{\nabla} S_{mix}) + \frac{\partial}{\partial y}\left(\frac{(E-P)S_{mix}}{H}\right) - \frac{\partial}{\partial y}\left(\frac{\Delta S}{H} w_e\right) + (res). \quad (3)$$

In this study, the temporal derivative $\partial/\partial t$ is estimated using the central difference scheme, and the meridional derivative $\partial/\partial y$ is calculated as the meridional difference between monthly climaotlogies averaged within artificial boxes on the 4° southern/higher and northern/lower salinity sides of the monthly climatological front in 150°–140°W. We note that positive and negative values indicate frontogenesis and frontolysis, respectively. The frontogenesis rate term [the left-hand side (LHS) term of Eq. (3)] shows reinforcement and relaxation of the SSS front in April–June and July–March, respectively (Fig. 4), which is broadly consistent with the seasonality of the intensity (Fig. 3). The ageostrophic advection and freshwater flux gradient terms [the first and second terms on the RHS of Eq. (3), respectively] contribute to frontogenesis throughout the year, while the entrainment gradient term [the third term on the RHS of Eq. (3)] acts as frontolysis in September–February when the mixed layer deepens on the both sides of the front. Although the residual term [the last term on the RHS of Eq. (3)] has substantial impacts on frontogenesis/frontolysis, further investigations await future works as discussed in the last section. In Section 3.2–3.4, the detail of the frontogenesis by the

ageostrophic advection and freshwater flux gradient terms and the frontolysis by the entrainment gradient term is described.

3.2 The ageostrophic advection gradient term

The ageostrophic advection gradient term [the first term on the RHS of Eq. (3)] can be decomposed as

$$-\frac{\partial}{\partial y}(\boldsymbol{u}^{\boldsymbol{a}}_{\boldsymbol{mix}}\cdot\boldsymbol{\nabla}S_{mix}) = -\frac{\partial u^a_{mix}}{\partial y}\frac{\partial S_{mix}}{\partial x} - u^a_{mix}\frac{\partial^2 S_{mix}}{\partial x\partial y} - \frac{\partial v^a_{mix}}{\partial y}\frac{\partial S_{mix}}{\partial y} - v^a_{mix}\frac{\partial^2 S_{mix}}{\partial y^2}. \quad (4)$$

Each term on the RHS denotes contributions from MLS advection by zonal shear and meridional convergence [the first and third terms on the RHS of Eq. (4), respectively] and zonal and meridional advection of the MLS gradient [the second and fourth terms on the RHS of Eq. (4), respectively]. Figure 5 shows that the meridional convergence term [the third term on the RHS term of Eq. (4)] has the dominant contribution to the ageostrophic advection gradient term [the LHS term of Eq. (4)], while the other terms is negligible. Although the horizontal Ekman advection consists of the horizontal Ekman transport and MLD [Eq. (2)], the meridional ageostrophic convergence is dominantly caused by the meridional Ekman transport gradient (figure not shown). Figure 6 shows westerly and easterly wind north and south of the center of the subtropical high, respectively. As is clear from Eq. (2), the meridional shears of zonal wind induce meridional convergence of the meridional Ekman transport. Higher salinity water is meridionally advected on the southern

234 side compared with the northern side, and therefore the ageostrophic advection
235 contributes to frontogenesis.
236
237 **3.3 The freshwater flux gradient term**
238 To investigate detailed mechanisms of the frontogenesis by the freshwater
239 flux gradient term [the second term on the RHS of Eq. (3)], we decompose it as
240

$$\frac{\partial}{\partial y}\left(\frac{(E-P)S_{mix}}{H}\right) = \frac{1}{H}\left(S_{mix}\frac{\partial E}{\partial y} - S_{mix}\frac{\partial P}{\partial y} + (E-P)\frac{\partial S_{mix}}{\partial y}\right) - \frac{(E-P)S_{mix}}{H^2}\frac{\partial H}{\partial y}. \quad (5)$$

241
242 Here, each term on the RHS indicates contributions from the gradients of
243 evaporation, precipitation, MLS, and MLD. While the MLS gradient term [the third
244 term on the RHS of Eq.(5)] has negligible small effects, the evaporation and
245 precipitation gradient terms [the first and second terms on the RHS of Eq. (5),
246 respectively] cause frontogenesis throughout the year (Fig. 7). The evaporation
247 gradient term shows a maximum peak in June–August, and the precipitation
248 gradient term has double minimum peaks in July and February. Although one may
249 think that contributions from freshwater fluxes are determined by only evaporation
250 and precipitation, the MLD gradient term [the last term on the RHS of Eq. (5)] has
251 substantial impacts on frontolysis and weakening the frontogenesis by the
252 evaporation and precipitation gradient terms in June–November.
253 The rate of evaporation on the southern side of the front is higher than the
254 northern side (Figs. 8a and 9), and thus the evaporation gradient term acts as

frontogenesis throughout the year. Using $E = Q_{lh}/\rho_f L$ and the aerodynamic bulk formula (e.g. Fairall et al. 1996), the evaporation gradient can be expressed as

$$\frac{\partial E}{\partial y} = \frac{1}{\rho_f L}\frac{\partial}{\partial y}\{C_{lh}u_{10}(q_s - q_a)\}$$
$$= \frac{1}{\rho_f L}\left\{u_{10}(q_s - q_a)\frac{\partial C_{lh}}{\partial y} + C_{lh}(q_s - q_a)\frac{\partial u_{10}}{\partial y} + C_{lh}u_{10}\frac{\partial q_s}{\partial y} - C_{lh}u_{10}\frac{\partial q_a}{\partial y}\right\} \quad (6)$$
$$+(res).$$

Here, $C_{lh} = \rho_a C_e L$, where ρ_a is the air density and C_e is the transfer coefficient of latent heat, u_{10} is wind speed at 10 m, q_s is surface saturated specific humidity, q_a is surface air specific humidity, and (res) denotes the residual term including sub-monthly terms. In this study, C_{lh} is calculated by dividing Q_{lh} by $u_{10}(q_s - q_a)$ using daily data. The coefficient and wind speed gradient terms [the first and second terms on the RHS of Eq. (6), respectively] as well as the residual term [the last term on the RHS of Eq. (6)] have minor influence on the evaporation gradient [the LHS term of Eq. (6)] (Fig. 10). The surface saturated specific humidity gradient is larger than the air specific humidity gradient throughout the year, and therefore the surface saturated specific humidity gradient term [the third term on the RHS of Eq. (6)] is dominant for the evaporation gradient [the LHS term of Eq. (6)]. Since surface saturated specific humidity is almost determined by SSTs, the SST gradient induces the evaporation gradient through the formation of the surface saturated specific humidity gradient. Although the evaporation gradient in winter has comparable values to summer (Fig. 10), the evaporation gradient term becomes small in winter (Fig. 7), because the seasonally thick mixed layer is less sensitive to evaporation (Fig.

8c).

The precipitation rate is low from the center to the southeastern side of the subtropical high in the North Pacific (e.g. Rodwell and Hoskins 2001; Miyasaka and Nakamura 2005; Fig. 11). As a result, it is lower on the southern side of the front than northern side (Fig. 8b), and thus the precipitation gradient term contributes to frontogenesis (Fig. 7). In summer, the subtropical high is strengthened and shifted northwestward, and both sides of the SSS front are covered with the low precipitation leading to weak frontogenesis by the precipitation gradient. Although the precipitation gradient is substantial in the other seasons, low sensitivity of the wintertime thick mixed layer to freshwater fluxes causes weak frontogenesis (Fig. 8c). Therefore, combination of the small precipitation gradient in summer and the thick mixed layer in winter results in double minimum peaks of the frontogenesis.

On the southern side of the front, the thicker mixed layer with less sensitivity to freshwater fluxes is distributed throughout the year (Figs. 8c, 12). Since the rate of evaporation exceeds that of precipitation around the SSS front in June–November (Figs. 8a, b), the MLD gradient induces frontolysis. In late winter, the mixed layer is seasonally thick and less sensitive to freshwater fluxes, and thus the MLD gradient has small influences on frontogenesis/frontolysis. Toyoda et al. (2004) pointed out that deep mixed layer in the ESTMW formation region south of the front results from northward advection of high salinity water by the meridional ageostrophic convergence and weak summertime heat fluxes caused by the presence of stratus cloud. Therefore, the MLD gradient has substantial impacts on not only SST but also SSS frontogenesis/frontolysis (e.g. Ohishi et al. 2016; Tozuka et al. 2017).

3.4 The entrainment gradient term

The entrainment gradient term [the third term on the RHS of Eq. (3)] can be decomposed as

$$-\frac{\partial}{\partial y}\left(\frac{\Delta S}{H}w_e\right) = -\frac{w_e}{H}\frac{\partial \Delta S}{\partial y} - \frac{\Delta S}{H}\frac{\partial w_e}{\partial y} + \frac{\Delta S w_e}{H^2}\frac{\partial H}{\partial y}, \quad (7)$$

where each term on the RHS represents effects from the salinity difference, entrainment velocity, and MLD gradients. Figure 13 shows that the salinity difference gradient term [the first term on the RHS of Eq. (7)] is dominant for the entrainment gradient term [the LHS term of Eq. (7)], while the entrainment velocity and MLD gradient terms [the second and third terms on the RHS of Eq. (7), respectively] have minor influence. On the southern side of the front, higher salinity water is distributed within the mixed layer than the lower layer (figure not shown) and the salinity difference between the mixed and entrained water is larger (Fig. 14). Based on the ventilated thermocline theory (Luyten et al. 1983), the low salinity water in the subsurface layer might origin from higher latitude regions through subduction processes. The mixed layer entrains lower salinity water from the lower layer south of the front during the entrainment phase, and therefore the salinity difference gradient relaxes the SSS front.

4. The freshwater flux frontogenesis metric

As described in Section 1, Tozuka et al. (2018) proposed "the heat flux frontogenesis metric" to quantify the relative importance of the horizontal gradient

of NHF and MLD for reinforcement/relaxation of that of MLTs, and revealed that the horizontal MLD gradient have dominant contributions in about 40–50% areas in the global ocean (see their Fig. 4). It is shown that the MLD gradient also has substantial impacts on the salinity frontogenesis/frontolysis as described in Section 3.3. In this section, we extend the results associated with the SSS frontogenesis/frontolysis in the northeastern Pacific to the global ocean by establishing the freshwater flux frontogenesis metric M to quantify the relative importance of the horizontal gradient of freshwater fluxes and MLD following the heat flux frontogenesis metric (Tozuka et al. 2018):

$$M = \arctan(G_{E-P} + G_H, G_{E-P} - G_H), \tag{8}$$

where

$$G_{E-P} = \nabla\{(E-P)S_{mix}\} \cdot \frac{\boldsymbol{\nabla} S_{mix}}{|\boldsymbol{\nabla} S_{mix}|} \tag{9}$$

and

$$G_H = -\frac{(E-P)S_{mix}}{H} \nabla H \cdot \frac{\boldsymbol{\nabla} S_{mix}}{|\boldsymbol{\nabla} S_{mix}|}. \tag{10}$$

G_{E-P} represents contribution from the horizontal freshwater flux gradient to reinforcement/relaxation of the horizontal MLS gradient when the MLD is assumed to be spatially uniform, and G_H denotes the corresponding effect of the horizontal

342 MLD gradient. M is an indicator how freshwater fluxes strengthen/weaken the
343 horizontal MLS gradient in its maximum direction (Fig. 15). When 0°<M<90° and –
344 90°<M<–180°, reinforcement and relaxation of the horizontal gradient of MLS by
345 that of freshwater fluxes (G_{E-P} frontogenesis and frontolysis) exceed effects from
346 that of MLD, respectively. Since the horizontal MLD gradient induces the difference
347 of mixed-layer sensitivity to freshwater fluxes leading to frontogenesis/frontolysis,
348 90°< M <180° and –90°< M <0° represent the corresponding reinforcement and
349 relaxation effects by the horizontal MLD gradient (G_H frontogenesis and
350 frontolysis) to G_{E-P} frontogenesis and frontolysis, respectively.

351 Horizontal distribution of M shows that distribution of each category is
352 geographically and temporally variable (Fig. 16). G_{E-P} frontogenesis and
353 frontolysis are more broadly distributed in the global ocean compared with G_H
354 frontogenesis and frontolysis. In both Hemispheres throughout the year, G_{E-P}
355 frontogenesis has the highest coverage of about 40–50 % among the four categories
356 (Figs. 17a, b), G_{E-P} frontolysis has the second highest coverage of about 30%, and
357 thus the total coverage of G_{E-P} frontogenesis and frontolysis reaches about 70–
358 80%. It means that the freshwater flux gradient plays the dominant roles in the
359 reinforcement/relaxation processes by freshwater fluxes in broad areas. In contrast,
360 G_H frontogenesis and frontolysis can be detected in the eastern subtropical regions,
361 where the subtropical high overlies and freshwater fluxes have relatively uniform
362 spatial pattern (c.f. Figs. 9, 11), and their coverage is small of 10–20% in both
363 Hemispheres for all months. G_{E-P} frontogenesis has seasonality of slightly larger
364 coverage in summer–autumn, while G_H frontogenesis and frontolysis show the
365 opposite seasonality (Figs. 17a, b).

366 Even if the analysis area is limited to frontal regions where the horizontal
367 SSS gradient magnitude is larger than 0.2 $(100\text{km})^{-1}$, qualitatively the similar results
368 are obtained in almost months (Figs. 17c, d). Although frontal regions in western
369 boundary currents and their extension regions are dominated by G_{E-P}
370 frontogenesis, G_{E-P} and G_H frontolysis have substantial impacts in the equatorial
371 Pacific region in boreal summer and the subtropical Atlantic region in boreal winter,
372 respectively (Fig. 16).
373 The freshwater flux frontogenesis metric indicates that the horizontal
374 gradient of the freshwater fluxes has the largest coverage, while that of the MLD is
375 minor. In contrast, the heat flux frontogenesis metric (Tozuka et al. 2018) shows that
376 the horizontal gradient of the MLD has comparable coverage to that of the heat fluxes.
377 We note that contributions of the horizontal gradient of the MLD to salinity
378 frontogenesis/frontolysis cannot be negligible, because it is dominant in eastern
379 subtropical regions (Fig. 16), and because it has substantial roles in damping the
380 frontogenesis by the horizontal freshwater flux gradient in the northeastern
381 subtropical Pacific region as described in Section 3.3.
382
383 **5. Conclusions**
384 SSS fronts play important roles to the ocean interior structure (Cronin and
385 McPhaden 2002; Katsura et al. 2015; Katsura 2018). This study has investigated the
386 quantitative nature of salinity frontogenesis/frontolysis in the northeastern
387 subtropical Pacific region where the horizontal gradient of SSS forms that of SSD. We
388 have used observational datasets to show that single strong and stable SSS front is
389 located in (150°–140°W, 30°–35°N) (Fig. 2) and undergoes a seasonal variation of

stronger and weaker intensity in summer and winter, respectively (Fig. 3). It is found that the ageostrophic advection and freshwater flux gradients strengthen the SSS front throughout the year, while the entrainment gradient acts as frontolysis during the mixed-layer deepening phase (Fig. 4). These processes are summarized in Fig. 18.

Meridional shears of zonal wind with westerly and easterly wind north and south of the subtropical high induce meridional ageostrophic convergence (Figs. 5, 6). Since the higher salinity water is meridionally advected on the southern side of the front than the northern side, the ageostrophic advection leads to frontogenesis throughout the year.

The SST gradient induces the evaporation gradient through the formation of the saturated specific humidity gradient in all months (Fig. 10). As a result, the rate of evaporation on the southern side of the front is higher than the northern side (Figs. 8a, 9), and thus the evaporation gradient causes frontogenesis (Fig. 7). In addition, the rate of precipitation is lower on the southern side of the front where the subtropical high overlies (Figs. 8b, 11), and thus the precipitation gradient acts as frontogenesis (Fig. 7). In the southern region, the mixed layer is thicker than the northern region and has less sensitivity to freshwater fluxes (Figs. 8c, 12). In June–November when the mixed layer is seasonally shallow and evaporation surpasses precipitation in the frontal region, the MLD gradient has substantial contributions to frontolysis and weakens the frontogenesis by the evaporation and precipitation gradients (Fig. 7).

On the southern side of the front, salinity within the mixed layer is higher and salinity difference between the mixed and entrained layer is larger (Fig. 14). In

September–February when the mixed layer deepens on both sides of the front, the mixed layer south of the front entrains lower salinity water from the lower layer, and thus the entrainment term contributes to frontolysis (Fig. 13).

We have proposed the freshwater flux frontogenesis metric [Eq. (8)] that is able to quantify the relative importance of the horizontal freshwater flux and MLD gradients in the global ocean (Fig. 15). G_{E-P} frontogenesis and frontolysis are broadly distributed in the global ocean, while G_H frontogenesis and frontolysis can be detected in eastern subtropical regions where freshwater fluxes have relatively uniform spatial pattern (Fig. 16). As also discussed in Tozuka et al. (2018), the metric is useful for intercomparing the performance of coupled and ocean general circulation models under High Resolution Model Intercomparison Project (HighResMIP; Haarsma et al. 2016) and may provide some insights for their improvement.

This study has applied the previous method used for SST fronts (e.g. Ohishi et al. 2016, 2017) to the salinity front, and quantitatively estimated salinity frontogenesis/frontolysis for the first time. The present method can be used for other salinity fronts in western boundary currents and their extension regions and equatorial Pacific and Atlantic regions (Fig. 1b). This study has revealed some differences between temperature and salinity frontogenesis/frontolysis as follows. While the evaporation gradient contributes to salinity frontogenesis as described the above, it relaxes SST fronts because stronger evaporation on the warmer side causes stronger net cooling in winter and weaker net heating in summer (Ohishi et al. 2016; Ohishi et al. 2019). The heat and freshwater frontogenesis metrics show the different distribution and coverage of each four category. The horizontal

gradient of MLD has less contributions to that of MLS in the global ocean and frontal regions compared with that of MLTs. However, contributions from the horizontal MLD gradient for salinity frontogenesis/frontolysis cannot be negligible, because it might has substantial impacts on frontogenesis/frontolysis by the horizontal freshwater flux gradient.

The residual term in the frontogenesis rate equation [the last term on the RHS of Eq. (1)] shows substantial effects on frontoenesis/frontolysis (Fig. 4), and sub-monthly effects reported by Qiu et al. (2014) are not considered in this study. As shown in Appendix 2, contributions from the vertical diffusivity are relatively consistent well with the residual term, but there are still large residual values even if including them to the frontogenesis rate equation (figure not shown). Further investigations may be possible if ocean general circulation models can realistically simulate the salinity and MLD fields and conserve each term of the salinity budget equation at each timestep. Sensitivity experiments with and without frontogenesis processes (freshwater fluxes and/or advection) using ocean models could produce salinity fields with and without the front, respectively, and might give further insight for the relationship between the SSS front and ESTMW. Further studies in this direction are under way.

Acknowledgements

We are thankful to two anonymous reviewers for their constructive and useful comments. The authors are grateful to participants at the "Research Meetings on Air–Sea Interaction" in 2018 held as a part of the Collaborative Research Program of Institute for Space-Earth Environmental Research, Nagoya University for their

comments. The second author is supported by JSPS Overseas Research Fellowships.

Appendix 1: A metric to evaluate the relative contributions of the horizontal SST and SSS gradients for the horizontal SSD gradient

Figure A1 shows global distribution of metric M_{TS} that evaluates the relative importance of the horizontal SST T_s and SSS S_s gradients for the horizontal SSD ρ_s gradient (Johnson et al. 2012), as represented as follows:

$$M_{TS} = \arctan(G_T + G_S, G_T - G_S) \tag{A1}$$

, where

$$G_T = -\alpha \nabla T_s \cdot \frac{\nabla \rho_s}{|\nabla \rho_s|} \tag{A2}$$

and

$$G_S = \beta \nabla S_s \cdot \frac{\nabla \rho_s}{|\nabla \rho_s|} \tag{A3}$$

Here, α is the thermal expansion coefficient and β is the haline contraction coefficient. The SSD gradient is formed mainly by the SST gradient when $0° < M_{TS} < 90°$ and the SSS gradient when $90° < M_{TS} < 180°$. Around the SSS front in the northeastern subtropical Pacific region, higher and lower salinity water on the southern and northern sides of the front forms heavier and lighter water,

respectively, and thus the horizontal gradient of SSS forms that of SSD.

Appendeix2: Contributions from the vertical diffusivity to salinity frontogenesis/frontolysis

Contributions from the vertical diffusivity included in the residual term in the frontogenesis rate equation [the last term on the RHS of Eq. (3)] can be represented as

$$-\frac{\partial}{\partial y}\left(\frac{\kappa}{H}\frac{\partial S}{\partial z}\Big|_{z=-H}\right) = -\frac{\kappa}{H}\frac{\partial}{\partial y}\left(\frac{\partial S}{\partial z}\Big|_{z=-H}\right) + \frac{\kappa}{H^2}\frac{\partial S}{\partial z}\Big|_{z=-H}\frac{\partial H}{\partial y}, \quad \text{(A4)}$$

where κ is the vertical diffusivity coefficient and $\partial S/\partial z|_{z=-H}$ denotes the vertical salinity gradient at the base of mixed layer. Here, we use the assumption that vertical diffusivity $\kappa = 1 \times 10^{-4}\ m^2 s^{-1}$ (c.f. Cronin et al. 2015) is temporally and spatially uniform and $\partial S/\partial z|_{z=-H}$ is estimated from the salinity difference between mixed layer and 20m below the base of the mixed layer. Each term on the RHS of Eq. (A4) indicates contributions from the salinity stratification and MLD gradients. As shown in Fig. A2, the vertical diffusivity gradient term [the LHS term of Eq. (A4)] dominated by the stratification gradient term [the 1st term on the RHS of Eq. (A4)] induces frontolysis throughout the year. This means that on the southern side of the front with high and low salinity at the surface and subsurface layer, respectively, the stronger salinity stratification induces stronger vertical diffusivity and thus weakens the SSS front.

The vertical diffusivity gradient term relatively corresponds well with the residual term [the last term on the RHS of Eq. (3)]. However, vertical diffusivity

505 contains uncertainty and the assumption might not be appropriate. Even if including
506 the contribution from the vertical diffusivity, the residual term still remains large
507 (figure not shown).
508

509 **References**

510 Akima H (1970) A new method of interpolation and smooth curve fitting based on
511 local procedures. J Assoc Comput Mach 17:589–602. doi:
512 10.1145/321607.321609
513 Ando K, Kuroda Y (2002) Two modes of salinity and temperature variation in the
514 surface layer of the Pacific Warm Pool. J Oceanogr 58:599–609. doi:
515 10.1023/A:1021223028579
516 Bourlès B, Lumpkin R, McPhaden MJ, Hernandez F, Nobre P, Campos E, Yu L,
517 Planton S, Busalacchi A, Moura AD, Servain J, Trotte J (2008) The Pirata
518 Program: History, accomplishments, and future directions. Bull Am Meteorol
519 Soc 89:1111–1125. doi: 10.1175/2008BAMS2462.1
520 Cronin MF, McPhaden MJ (1998) Upper ocean salinity balance in the western
521 equatorial Pacific. J Geophys Res Ocean 103:27567–27587. doi:
522 10.1029/98JC02605
523 Cronin MF, McPhaden MJ (2002) Barrier layer formation during westerly wind
524 bursts. J Geophys Res Ocean 107:8020. doi: 10.1029/2001JC001171
525 Cronin MF, Pelland NA, Emerson SR, Crawford WR (2015) Estimating diffusivity
526 from the mixed layer heat and salt balances in the North Pacific. J Geophys Res
527 Ocean 120:7346–7362. doi: 10.1002/2015JC011010
528 Cronin MF, Tozuka T (2016) Steady state ocean response to wind forcing in
529 extratropical frontal regions. Sci Rep 6:28842. doi: 10.1038/srep28842
530 Ducet N, Le Traon PY, Reverdin G (2000) Global high-resolution mapping of ocean
531 circulation from TOPEX/Poseidon and ERS-1 and -2. J Geophys Res
532 105:19477–19498. doi: 10.1029/2000JC900063

533 Ekman VW (1905) On the influence of the earth's rotation on ocean-currents. Arch
534 Math Astron Phys 2:1–52.
535 Fairall CW, Bradley EF, Rogers DP, Edson JB, Young GS (1996) Bulk
536 parameterization of air-sea fluxes for Tropical Ocean-Global Atmosphere
537 Coupled-Ocean Atmosphere Response Experiment. J Geophys Res Ocean
538 101:3747–3764. doi: 10.1029/95JC03205
539 Foltz GR, Grodsky SA, Carton JA, McPhaden MJ (2004) Seasonal salt budget of the
540 northwestern tropical Atlantic Ocean along 38°W. J Geophys Res Ocean
541 109:C03052. doi: 10.1029/2003JC002111
542 Haarsma RJ, Roberts MJ, Vidale PL, Senior CA, Bellucci A, Bao Q, Chang P, Corti S,
543 Fučkar NS, Guemas V, von Hardenberg J, Hazeleger W, Kodama C, Koenigk T,
544 Leung LR, Lu J, Luo J-J, Mao J, Mizielinski MS, Mizuta R, Nobre P, Satoh M,
545 Scoccimarro E, Semmler T, Small J, von Storch J-S (2016) High Resolution
546 Model Intercomparison Project (HighResMIP v1.0) for CMIP6. Geosci Model
547 Dev 9:4185–4208. doi: 10.5194/gmd-9-4185-2016
548 Hautala SL, Roemmich DH (1998) Subtropical mode water in the northeast Pacific
549 basin. J Geophys Res Ocean 103:13055–13066. doi: 10.1029/98JC01015
550 Johnson GC, Schmidtko S, Lyman JM (2012) Relative contributions of temperature
551 and salinity to seasonal mixed layer density changes and horizontal density
552 gradients. J Geophys Res Ocean 117:C04015. doi: 10.1029/2011JC007651
553 Kao H-Y, Lagerloef GSE (2015) Salinity fronts in the tropical Pacific Ocean. J
554 Geophys Res Ocean 120:1096–1106. doi: 10.1002/ 2014JC010114
555 Katsura S (2018) Properties, formation, and dissipation of the North Pacific
556 Eastern Subtropical Mode Water and its impact on interannual spiciness

anomalies. Prog Oceanogr 162:120–131. doi: 10.1016/j.pocean.2018.02.023

Katsura S, Oka E, Qiu B, Schneider N (2013) Formation and subduction of North Pacific Tropical Water and their interannual variability. J Phys Oceanogr 43:2400–2415. doi: 10.1175/JPO-D-13-031.1

Katsura S, Oka E, Sato K (2015) Formation mechanism of barrier layer in the subtropical Pacific. J Phys Oceanogr 45:2790–2805. doi: 10.1175/JPO-D-15-0028.1

Kobayashi S, Ota Y, Harada Y, Ebita A, Moriya M, Onoda H, Onogi K, Kamahori H, Kobayashi C, Endo H, Miyaoka K, Takahashi K (2015) The JRA-55 reanalysis: General specifications and basic characteristics. J Meteorol Soc Japan 93:5–48. doi: 10.2151/jmsj.2015-001

Konda M, Ichikawa H, Tomita H, Cronin MF (2010) Surface heat flux variations across the Kuroshio Extension as observed by surface flux buoys. J Clim 23:5206–5221. doi: 10.1175/2010jcli3391.1

Luyten JR, Pedlosky J, Stommel H (1983) The ventilated thermocline. J Phys Oceanogr 13:292–309. doi: 10.1175/1520-0485(1983)013<0292:TVT>2.0.CO;2

McPhaden MJ (1995) The Tropical Atmosphere Ocean array is completed. Bull Am Meteorol Soc 76:739–741. doi: 10.1080/00420980220128363

Mecklenburg S, Drusch M, Kerr YH, Font J, Martin-Neira M, Delwart S, Buenadicha G, Reul N, Daganzo-Eusebio E, Oliva R, Crapolicchio R (2012) ESA's soil moisture and ocean salinity mission: Mission performance and operations. IEEE Trans Geosci Remote Sens 50:1354–1366. doi: 10.1109/TGRS.2012.2187666

581 Miyasaka T, Nakamura H (2005) Structure and formation mechanisms of the
582 Northern Hemisphere summertime subtropical highs. J Clim 18:5046–5065.
583 doi: 10.1175/JCLI3599.1
584 Niiler PP, Kraus EB (1977) One-dimensional models of the upper ocean. Pergamon
585 New York 143–172.
586 Ohishi S, Aiki H, Tozuka T, Cronin MF (2019) Frontolysis by surface heat flux in the
587 eastern Japan Sea: importance of mixed layer depth. J Oceanogr 75:283–297.
588 doi: 10.1007/s10872-018-0502-0
589 Ohishi S, Tozuka T, Cronin MF (2017) Frontogenesis in the Agulhas Return Current
590 region simulated by a high-resolution CGCM. J Phys Oceanogr 47:2691–2710.
591 doi: 10.1175/JPO-D-17-0038.1
592 Ohishi S, Tozuka T, Komori N (2016) Frontolysis by surface heat flux in the
593 Agulhas Return Current region with a focus on mixed layer processes:
594 observation and a high-resolution CGCM. Clim Dyn 47:3993–4007. doi:
595 10.1007/s00382-016-3056-0
596 Qiu C, Kawamura H, Mao H, Wu J (2014) Mechanisms of the disappearance of sea
597 surface temperature fronts in the subtropical North Pacific Ocean. J Geophys
598 Res Ocean 119:4389–4398. doi: 10.1002/2014JC010142
599 Ren L, Riser SC (2009) Seasonal salt budget in the northeast Pacific Ocean. J
600 Geophys Res Ocean 114:C12004. doi: 10.1029/2009JC005307
601 Rodwell MJ, Hoskins BJ (2001) Subtropical anticyclones and summer monsoons. J
602 Clim 14:3192–3211. doi: 10.1175/1520-
603 0442(2001)014<3192:SAASM>2.0.CO;2
604 Roemmich D, Johnson G, Riser S, Davis R, Gilson J, Owens WB, Garzoli S, Schmid C,

605 Ignaszewski M (2009) The Argo Program: Observing the Global Oceans with
606 Profiling Floats. Oceanography 22:34–43. doi: 10.5670/oceanog.2009.36
607 Schmidtko S, Johnson GC, Lyman JM (2013) MIMOC: A global monthly isopycnal
608 upper-ocean climatology with mixed layers. J Geophys Res Ocean 118:1658–
609 1672. doi: 10.1002/jgrc.20122
610 Tomita H, Hihara T, Kako S, Kubota M, Kutsuwada K (2019) An introduction to J-
611 OFURO3, a third-generation Japanese ocean flux data set using remote-
612 sensing observations. J Oceanogr 75:171–194. doi: 10.1007/s10872-018-
613 0493-x
614 Toyoda T, Awaji T, Ishikawa Y, Nakamura T (2004) Preconditioning of winter
615 mixed layer in the formation of North Pacific eastern subtropical mode water.
616 Geophys Res Lett 31:L17206. doi: 10.1029/2004GL020677
617 Tozuka T, Cronin MF (2014) Role of mixed layer depth in surface frontogenesis:
618 The Agulhas Return Current front. Geophys Res Lett 41:2447–2453. doi:
619 10.1002/2014GL059624
620 Tozuka T, Cronin MF, Tomita H (2017) Surface frontogenesis by surface heat fluxes
621 in the upstream Kuroshio Extension region. Sci Rep 7:10258. doi:
622 10.1038/s41598-017-10268-3
623 Tozuka T, Ohishi S, Cronin MF (2018) A metric for surface heat flux effect on
624 horizontal sea surface temperature gradients. Clim Dyn 51:547–561. doi:
625 10.1007/s00382-017-3940-2
626 Vialard J, Delecluse P (1998a) An OGCM study for the TOGA decade. Part I: Role of
627 salinity in the physics of the western Pacific fresh pool. J Phys Oceanogr
628 28:1071–1088. doi: 10.1175/1520-0485(1998)028<1071:AOSFTT>2.0.CO;2

Vialard J, Delecluse P (1998b) An OGCM study for the TOGA decade. Part II: Barrier-layer formation and variability. J Phys Oceanogr 28:1089–1106. doi: 10.1175/1520-0485(1998)028<1089:AOSFTT>2.0.CO;2

Webster PJ, Lukas R (1992) TOGA COARE: The Coupled Ocean—Atmosphere Response Experiment. Bull Am Meteorol Soc 73:1377–1416. doi: 10.1175/1520-0477(1992)073<1377:TCTCOR>2.0.CO;2

Yu L (2015) Sea-surface salinity fronts and associated salinity-minimum zones in the tropical ocean. J Geophys Res Ocean 120:4205–4225. doi: doi:10.1002/2015JC010790

Figure caption:

Fig. 1 (a) Annual mean of sea surface temperatures (SSTs; contour) and their horizontal gradient magnitude (color) estimated from the Monthly Isopycnal/Mixed-layer Ocean Climatology (MIMOC; Schmidtko et al. 2013). (b) As in (a), but for sea surface salinity (SSS). Thin (Thick) contour intervals are (a) 2 (10) °C and (b) 0.25 (1).

Fig. 2 Annual mean of (a) position and (b) intensity of the SSS front. Error bars denote standard deviations calculated from monthly climatologies. In (a), black contours and color shading represent annual mean of SSS and its horizontal gradient magnitude, respectively. Thin (Thick) contour intervals are 0.2 (1).

Fig. 3 Monthly climatology of intensity averaged within 150°–140°W where the SSS front is strong and stable. Note that the intensity is defined as a maximum of the horizontal SSS gradient magnitude in 25°–40°N at each longitude.

Fig. 4 Monthly climatology of each term of Eq. (3): the frontogenesis rate [the left-hand side (LHS) term; black bar], the ageostrophic advection gradient term [the first term on the right-hand side (RHS); green line], the freshwater flux advection gradient term (the second term on the RHS; red line), the entrainment gradient term (the third term on the RHS; blue line), and the residual term (the last term on the RHS; gray line). Note that when calculating the temporal derivative $\partial/\partial t$ the central difference method is used , and the meridional derivative $\partial/\partial y$ is calculated as the meridional difference between monthly climaotlogies averaged within artificial boxes on the 4° southern/higher and northern/lower salinity sides of the monthly climatological front in 150°–140°W.

Fig. 5 As in Fig. 4, but for Eq. (4): the ageostrophic advection gradient term (the LHS

term; black bar) and contributions from the zonal shear (the first term on the RHS; red line), the zonal advection of the mixed layer salinity (MLS) gradient (the second term on the RHS; orange line), the meridional convergence (the third term on the RHS; blue line), and the meridional advection of the MLS gradient term (the last term on the RHS; cyan line).

Fig. 6 Monthly climatology of the meridional Ekman transport (color), SSS (black contour), and sea level pressure (SLP; white contour) in (a) February, (b) May, (c) August, and (d) November. Thin (Thick) black and white contour intervals are 0.2 (1) and 2 (10) hPa, respectively.

Fig. 7 As in Fig. 4, but for Eq. (5): The freshwater flux gradient term (the LHS term; black bar), the evaporation gradient term (the first term on the RHS; orange line), the precipitation gradient term (the second term on the RHS; cyan line), the MLS gradient term (the third term on the RHS; yellow line), and the mixed layer depth (MLD) gradient term (the last term on the RHS; gray line).

Fig. 8 Monthly climatology of the rate of (a) evaporation and (b) precipitation, and (c) MLD on the southern (red line) and northern (blue line) sides of the front and their gradients (black bar). Note that the gradient indicates the difference of variables between on the southern and northern sides of the front.

Fig. 9 As in Fig. 6, but for the rate of evaporation (color and white contour). Thin (Thick) white contour intervals are 0.02 (0.1) m $month^{-1}$.

Fig. 10 As in Fig. 4, but for Eq. (6): the evaporation gradient (the LHS term; black bar), the coefficient gradient term (the first term on the RHS; yellow line), the wind speed gradient term (the second term on the RHS; green line), the surface saturated specific humidity term (the third term on the RHS; blue line), the air specific

687 humidity gradient term (the fourth term on the RHS; red line), and the residual term
688 (the last term on the RHS; gray line).
689 **Fig. 11** As in Fig. 6, but for precipitation (color) in (a) February, (b) May, (c) July, and
690 (d) September. Note that the precipitation gradient term [the second term on the
691 RHS of Eq. (5)] has maximal values in May and September and minimal values in
692 February and July.
693 **Fig. 12** As in Fig. 6, but for MLD (color and white contour). Thin (Thick) contour
694 intervals are 20 (100) m in (a) and 10 (50) m in (b)–(d).
695 **Fig. 13** As in Fig. 4, but for Eq. (7) in September–February when the mixed layer
696 deepens on both sides of the front: the entrainment gradient term (the LHS term;
697 black bar), the salinity difference gradient term (the first term on the RHS; orange
698 line), the entrainment velocity gradient term (the second term on the RHS; cyan line),
699 and the MLD gradient term (the third term on the RHS; gray line).
700 **Fig. 14** As in Fig. 6, but for the salinity difference between the mixed layer and
701 entrained water (color and white contour) in (a) September, (b) November, and (c)
702 January. Thin (Thick) white contour intervals are 0.1 (0.5).
703 **Fig. 15** A schematic diagram to illustrate the definition and physical interpretation
704 of the freshwater flux frontogenesis metric M [Eq. (8)]. The horizontal MLS
705 gradient is strengthened by the horizontal gradients of freshwater fluxes and MLD
706 (G_{E-P} and G_H frontogenesis) when $0°<M<90°$ and $90°<M<180°$, and relaxed by
707 those (G_{E-P} and G_H frontolysis) when $-90°< M <0°$ and $-180°< M <-90°$,
708 respectively.
709 **Fig. 16** Global map of the freshwater flux frontogenesis metric in (a) February and
710 (b) August. Yellow lines enclose regions with the horizontal SSS gradient magnitude

711 larger than 0.2 (100km)$^{-1}$.

712 **Fig. 17** Monthly percentage of areas covered with each category of the freshwater
713 flux frontogenesis metric in the (a) Northern and (b) Southern Hemispheres. (c), (d)
714 As in (a), (b), but for frontal regions where the horizontal SSS gradient magnitude is
715 larger than 0.2 (100km)$^{-1}$, respectively (see Fig. 16).

716 **Fig. 18** A schematic diagram of salinity frontogenesis by freshwater fluxes and
717 ageostrophic advection and frontolysis by entrainment during mixed-layer
718 deepening phase (September–February) in the northeastern subtropical Pacific
719 region. The upper red (blue) boxes represent mixed layers with high (low) salinity
720 water separated by the mixed layer depth (gray line), the dark red (blue) arrows in
721 the boxes indicate the meridional ageostrophic velocity. The light red (cyan) boxes
722 below the mixed-layer boxes have much lower (lower) salinity water, and the gray
723 vectors indicate mixed-layer deepening leading to the entrainment. Cyan (Orange)
724 cloud-shape objects denote surface saturated (air) specific humidity, and orange
725 vectors denote evaporation. Gray cloud-shape objects indicate the precipitation.

726 **Fig. A1** Global map of annual mean of sea surface density (SSD; contour) and a
727 metric M_{TS} [Eq. (A1); color] calculated from annual mean of SSTs, SSS, and SSD.
728 Yellow (Purple) contour lines enclose regions with the horizontal SST (SSS) gradient
729 magnitude larger than 1.5 °C (100 km)$^{-1}$ [0.2 (100 km)$^{-1}$]. Thin (Thick) contour
730 intervals are 0.25 (1) kg m^{-3}.

731 **Fig. A2** As in Fig.4, but for Eq. (A4): the vertical diffusivity gradient term (the LHS
732 term; black bar) and contributions from the salinity stratification (the first term on
733 the RHS; red line) and the MLD (the second term on the RHS; blue line). Gray line
734 denotes the residual term of the frontogenesis rate equation [the last term on the

735 RHS of Eq. (3)].

736

737 **Figures**

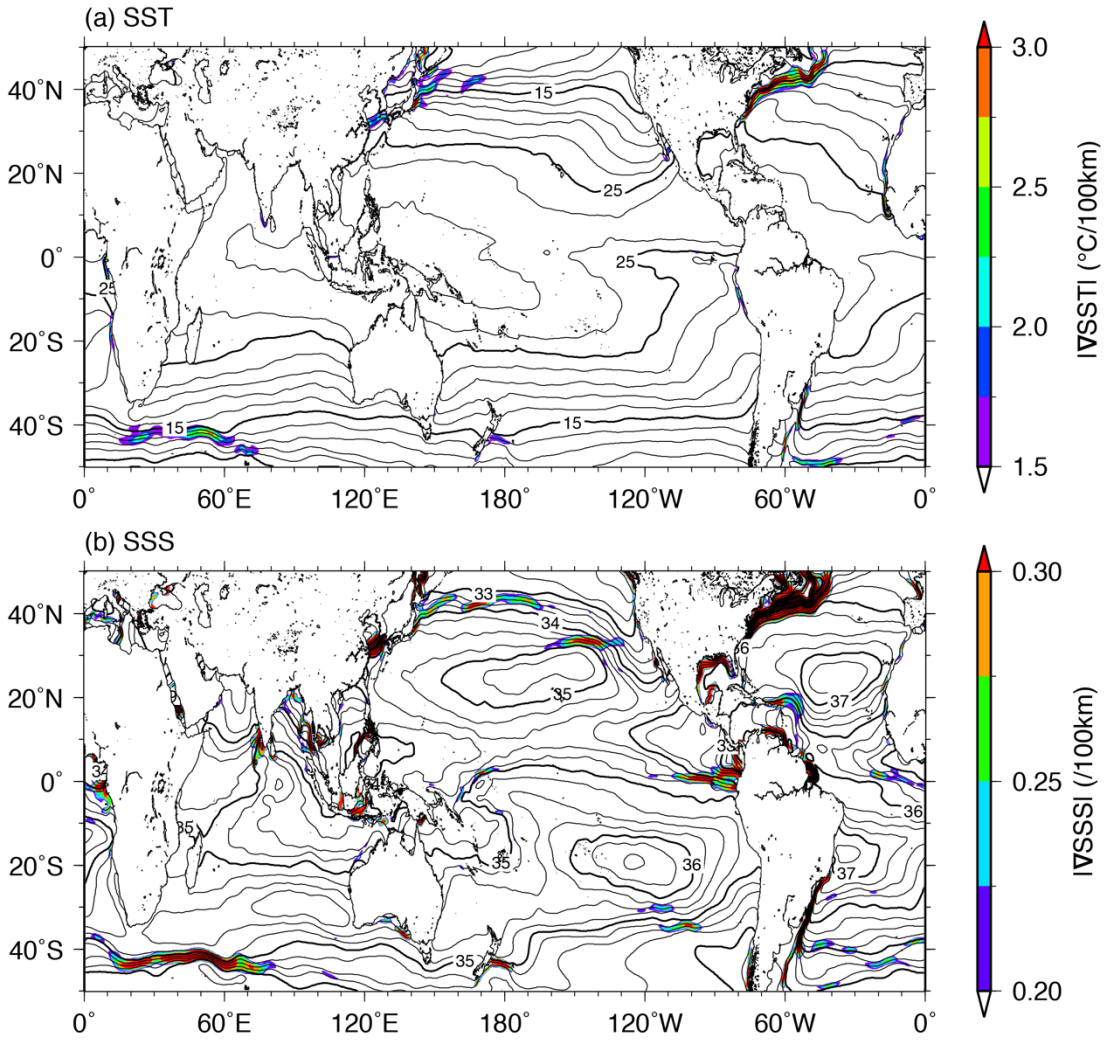

738

739 **Fig. 1** (a) Annual mean of sea surface temperatures (SSTs; contour) and their
740 horizontal gradient magnitude (color) estimated from the Monthly
741 Isopycnal/Mixed-layer Ocean Climatology (MIMOC; Schmidtko et al. 2013). (b) As in
742 (a), but for sea surface salinity (SSS). Thin (Thick) contour intervals are (a) 2 (10) °C
743 and (b) 0.25 (1).

744

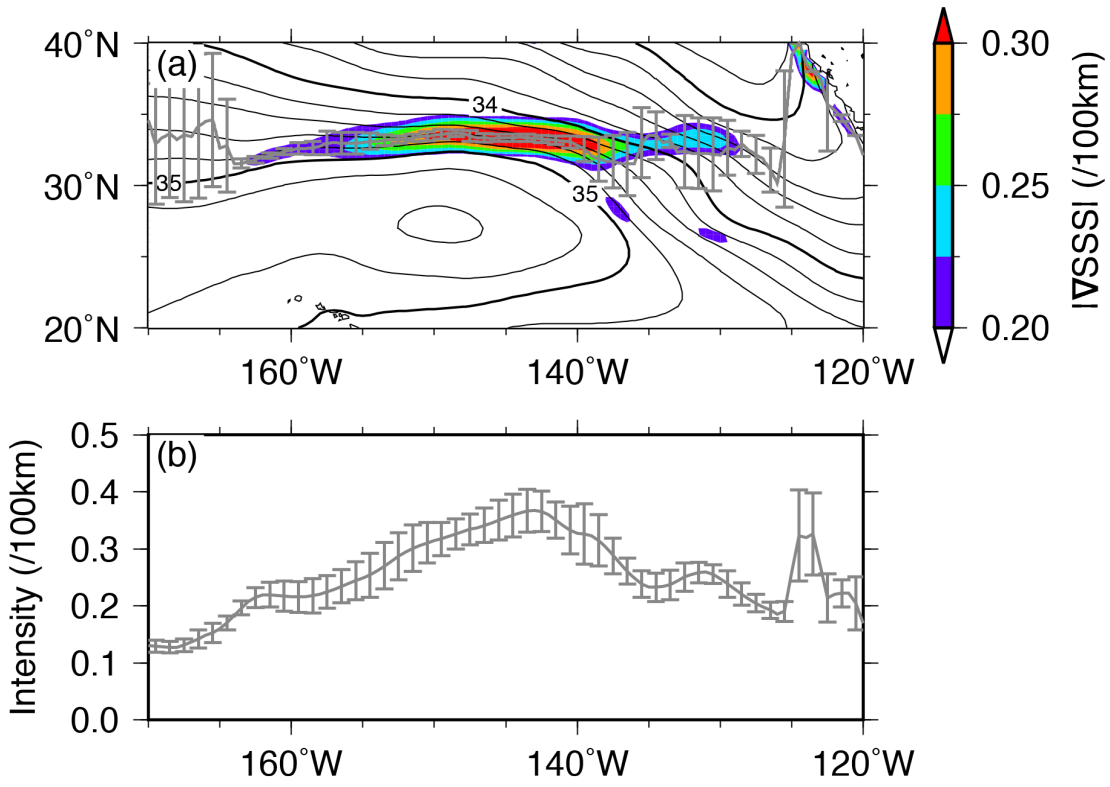

745

746 **Fig. 2** Annual mean of (a) position and (b) intensity of the SSS front. Error bars
747 denote standard deviations calculated from monthly climatologies. In (a), black
748 contours and color shading represent annual mean of SSS and its horizontal gradient
749 magnitude, respectively. Thin (Thick) contour intervals are 0.2 (1).

750

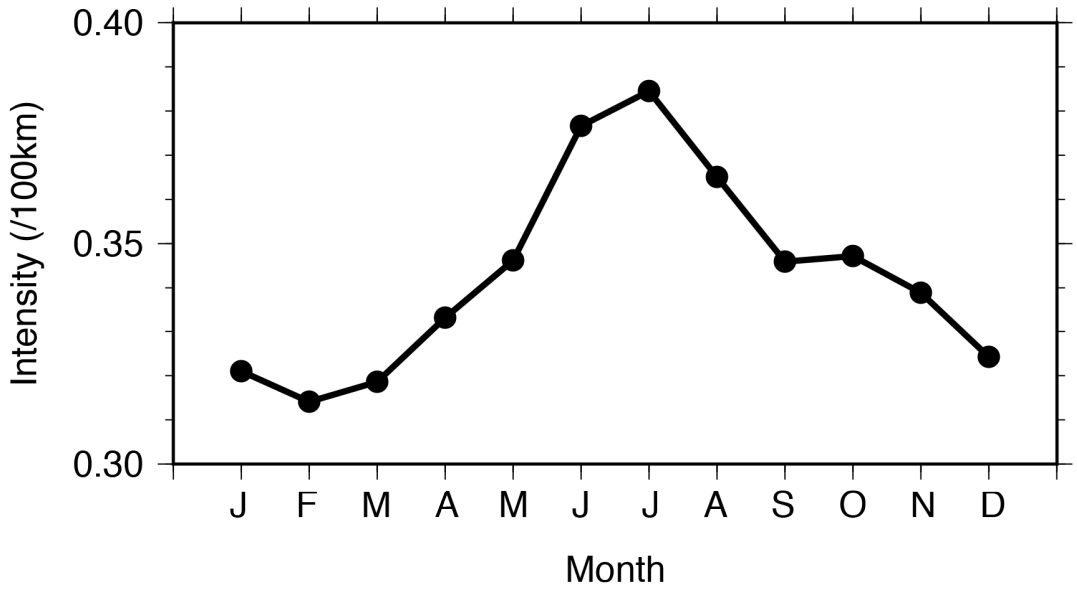

751

752 **Fig. 3** Monthly climatology of intensity averaged within 150°–140°W where the SSS

753 front is strong and stable. Note that the intensity is defined as a maximum of the

754 horizontal SSS gradient magnitude in 25°–40°N at each longitude.

755

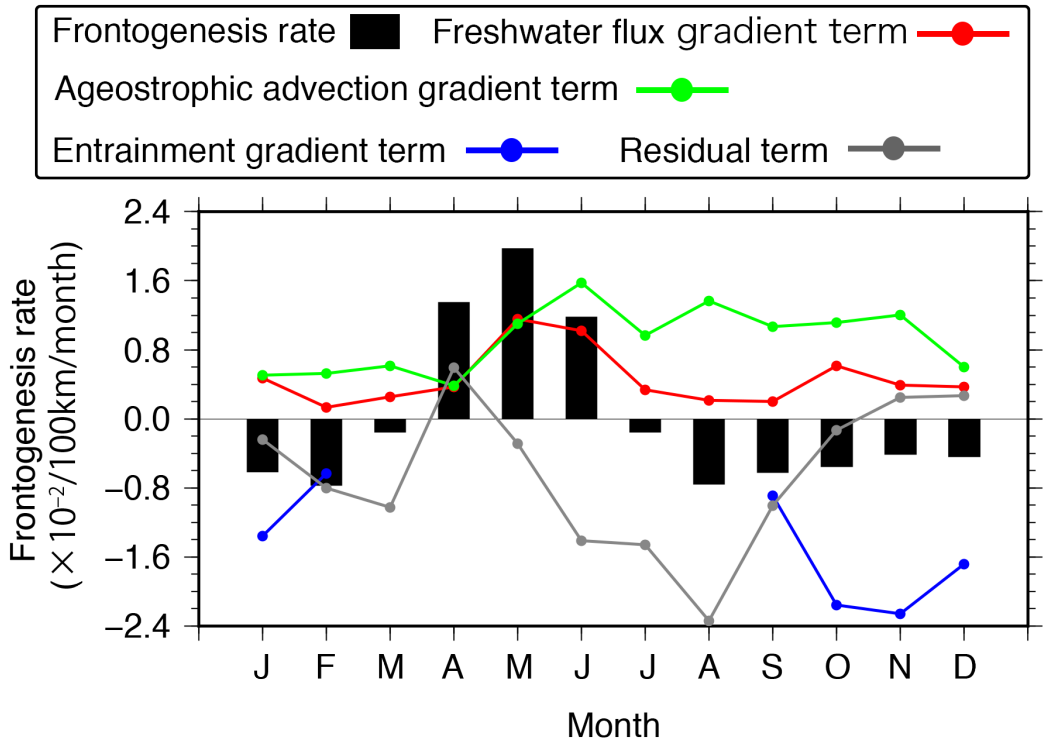

Fig. 4 Monthly climatology of each term of Eq. (3): the frontogenesis rate [the left-hand side (LHS) term; black bar], the ageostrophic advection gradient term [the first term on the right-hand side (RHS); green line], the freshwater flux advection gradient term (the second term on the RHS; red line), the entrainment gradient term (the third term on the RHS; blue line), and the residual term (the last term on the RHS; gray line). Note that when calculating the temporal derivative $\partial/\partial t$ the central difference method is used , and the meridional derivative $\partial/\partial y$ is calculated as the meridional difference between monthly climaotlogies averaged within artificial boxes on the 4° southern/higher and northern/lower salinity sides of the monthly climatological front in 150°–140°W.

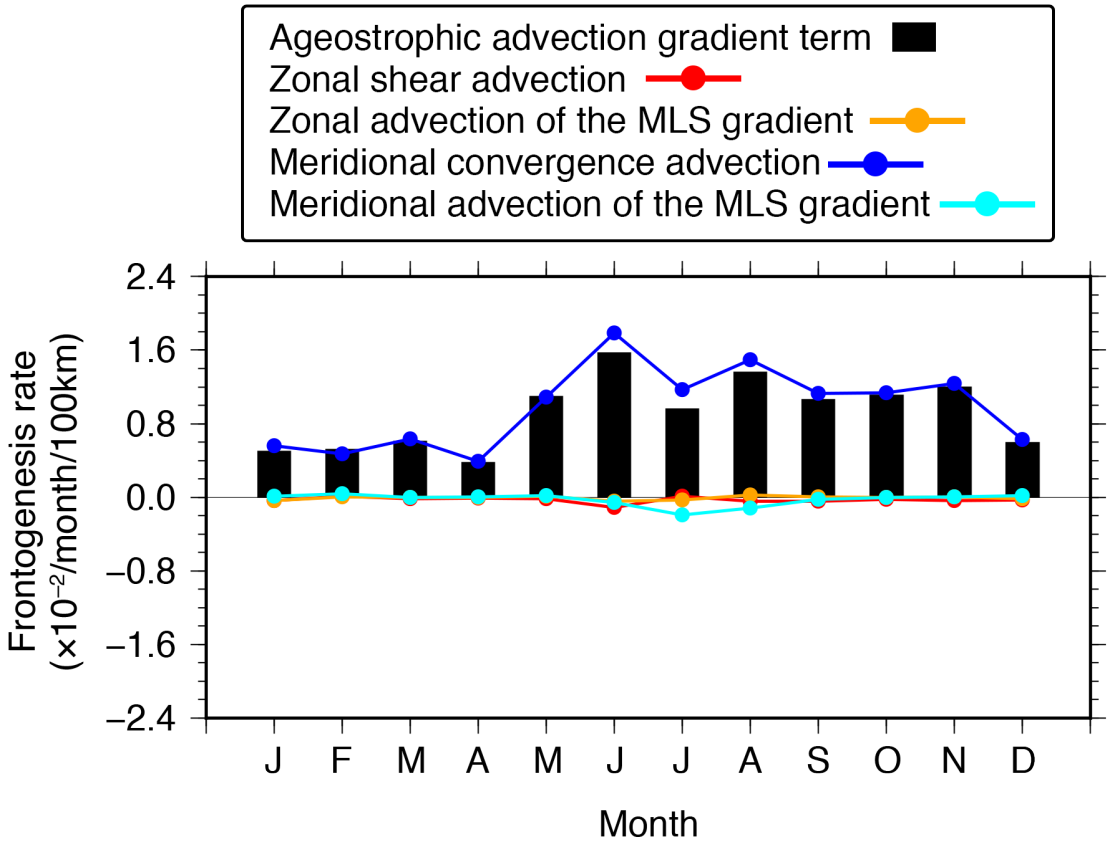

768

769 **Fig. 5** As in Fig. 4, but for Eq. (4): the ageostrophic advection gradient term (the LHS
770 term; black bar) and contributions from the zonal shear (the first term on the RHS;
771 red line), the zonal advection of the mixed layer salinity (MLS) gradient (the second
772 term on the RHS; orange line), the meridional convergence (the third term on the
773 RHS; blue line), and the meridional advection of the MLS gradient term (the last term
774 on the RHS; cyan line).

775

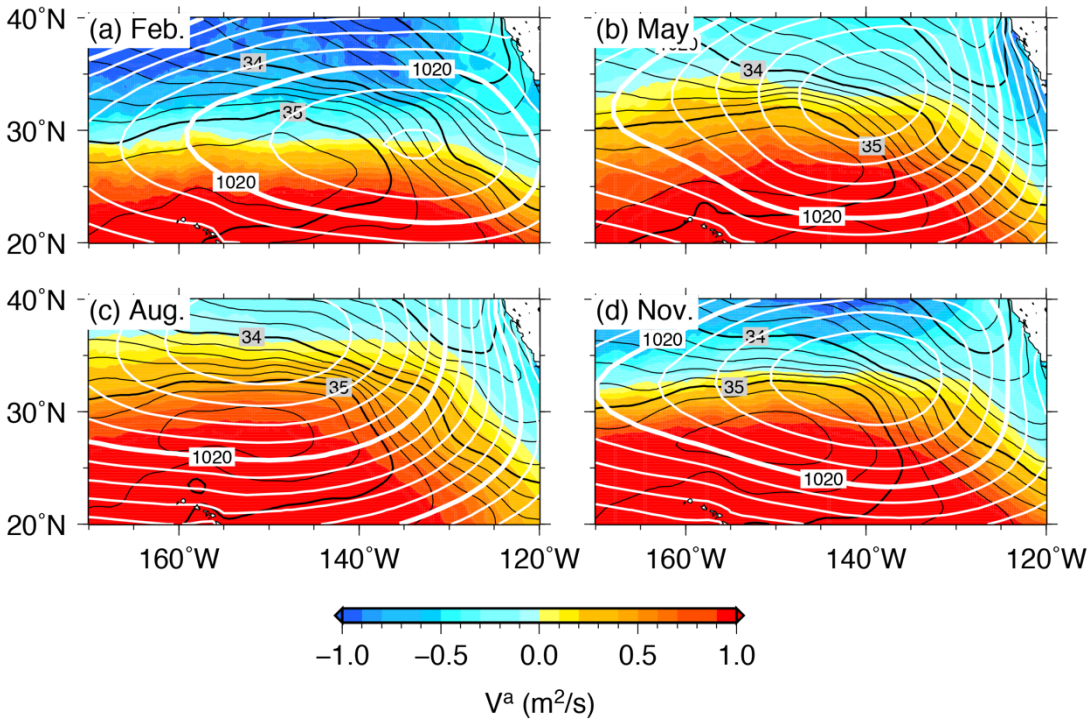

776

777 **Fig. 6** Monthly climatology of the meridional Ekman transport (color), SSS (black
778 contour), and sea level pressure (SLP; white contour) in (a) February, (b) May, (c)
779 August, and (d) November. Thin (Thick) black and white contour intervals are 0.2
780 (1) and 2 (10) hPa, respectively.

781

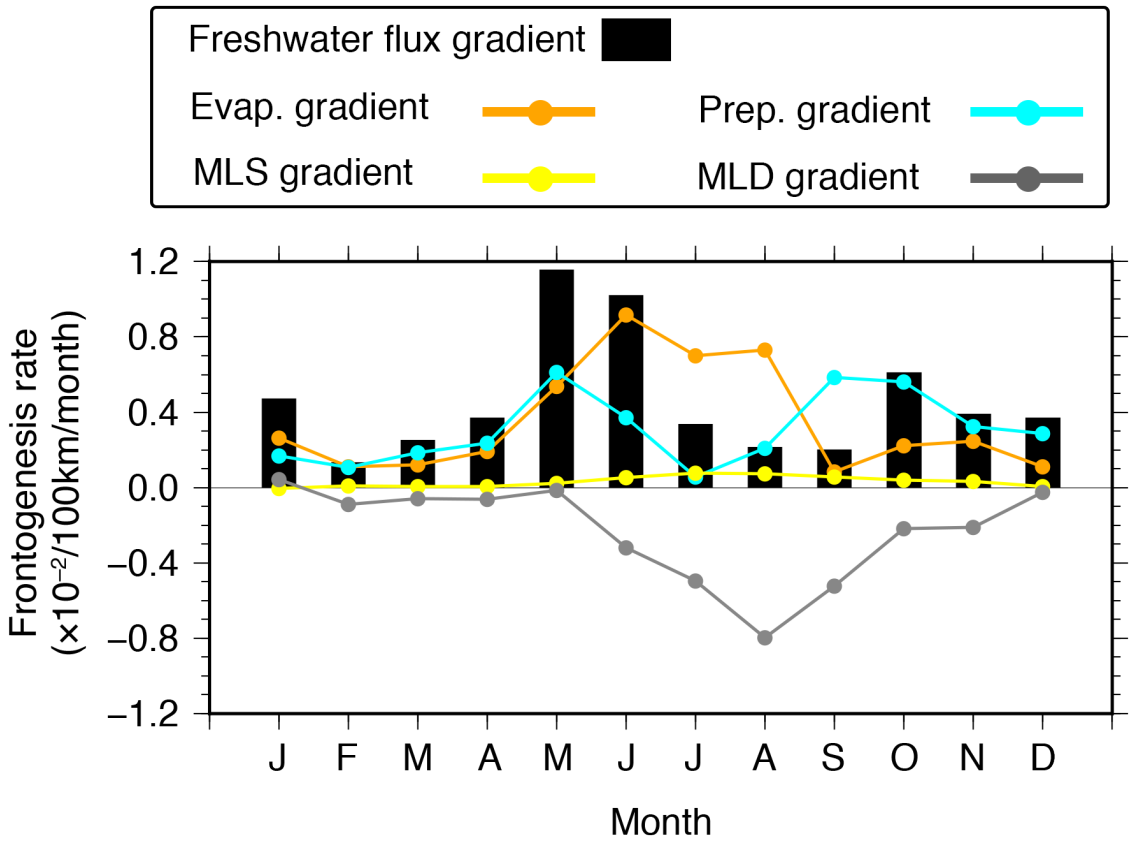

782

783 **Fig. 7** As in Fig. 4, but for Eq. (5): The freshwater flux gradient term (the LHS term;
784 black bar), the evaporation gradient term (the first term on the RHS; orange line),
785 the precipitation gradient term (the second term on the RHS; cyan line), the MLS
786 gradient term (the third term on the RHS; yellow line), and the mixed layer depth
787 (MLD) gradient term (the last term on the RHS; gray line).

788

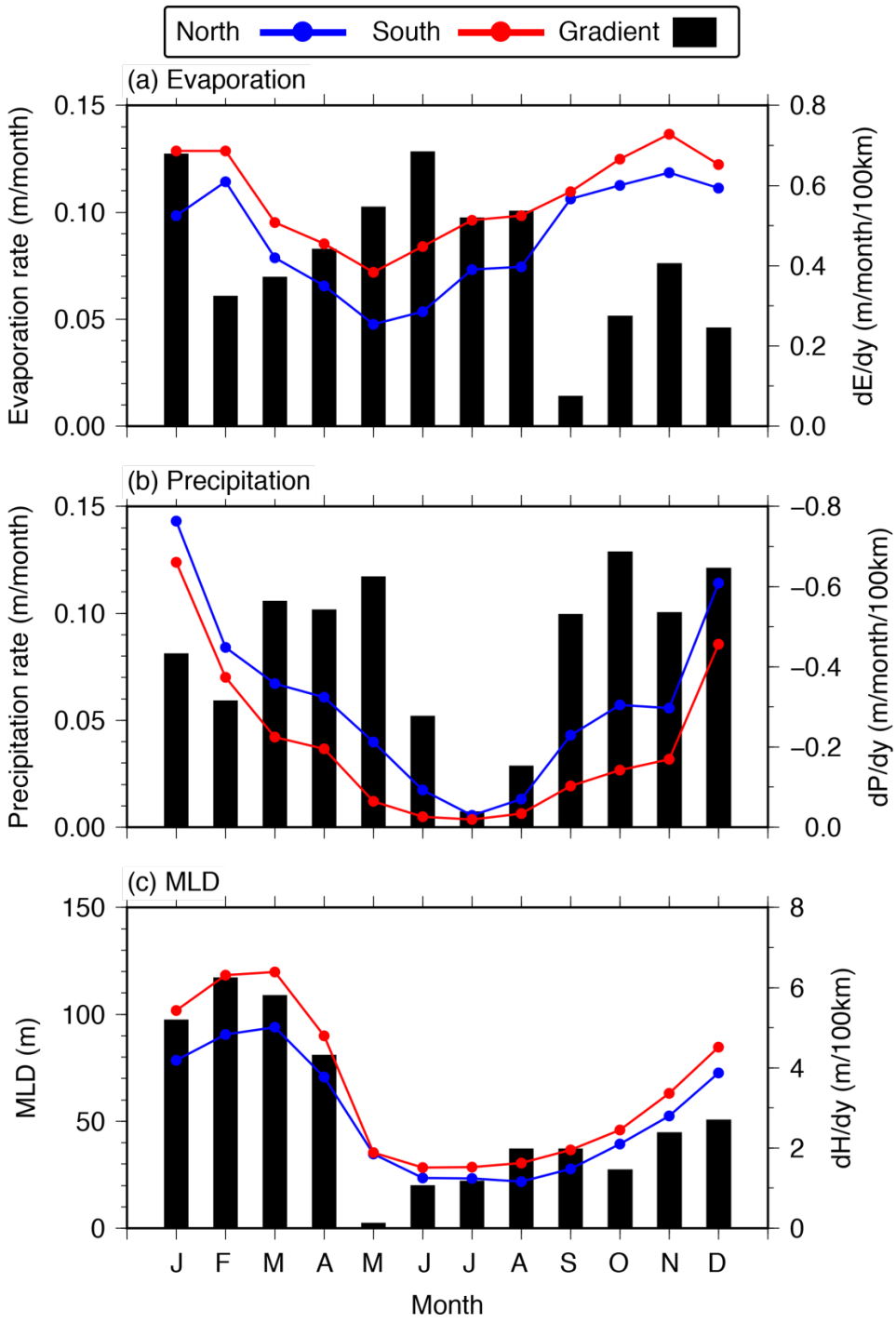

789

790 **Fig. 8** Monthly climatology of the rate of (a) evaporation and (b) precipitation, and
791 (c) MLD on the southern (red line) and northern (blue line) sides of the front and
792 their gradients (black bar). Note that the gradient indicates the difference of
793 variables between on the southern and northern sides of the front.

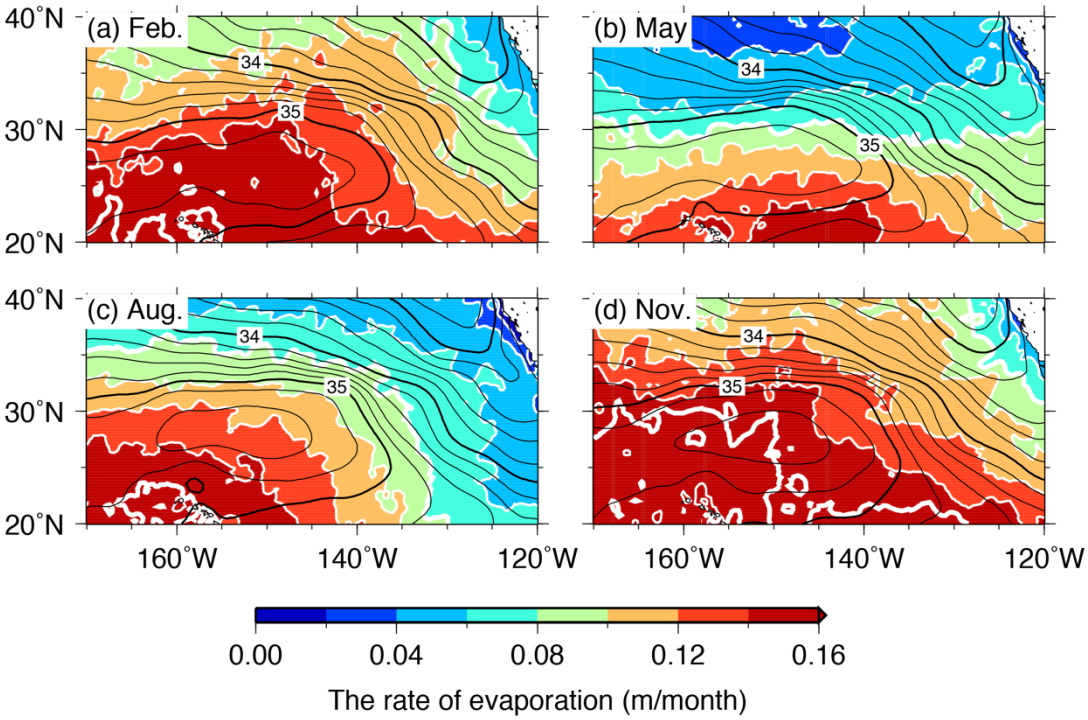

794

795 **Fig. 9** As in Fig. 6, but for the rate of evaporation (color and white contour). Thin

796 (Thick) white contour intervals are 0.02 (0.1) m month^{-1}.

797

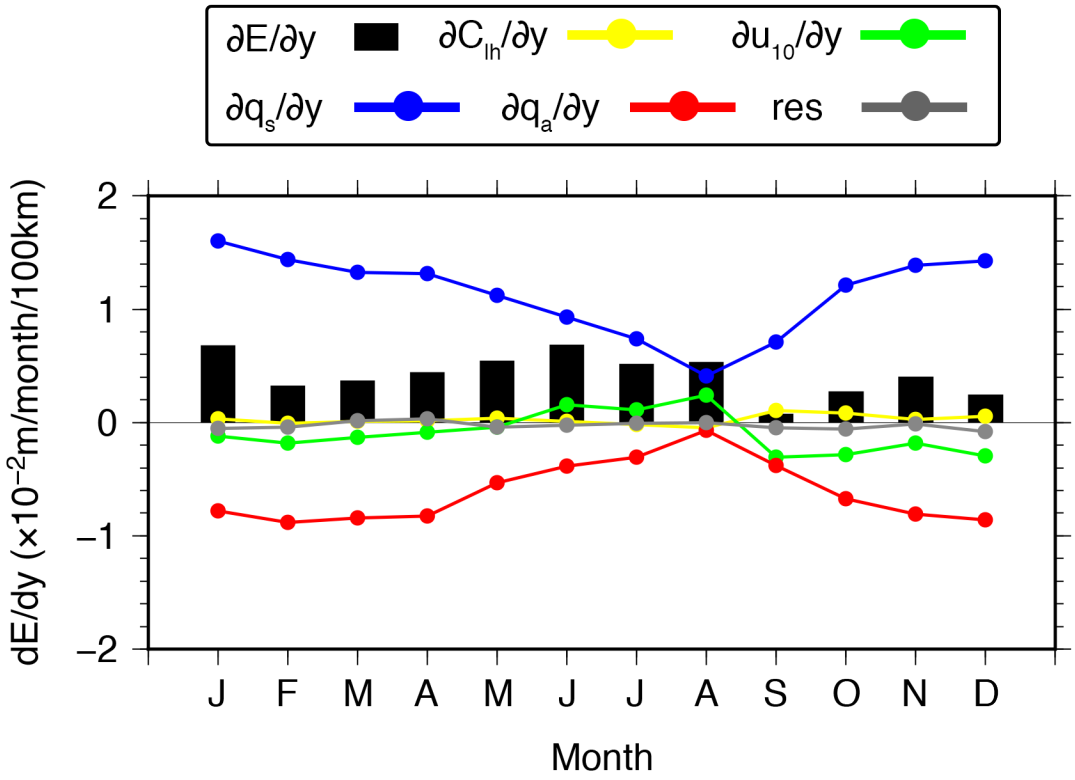

798

799 **Fig. 10** As in Fig. 4, but for Eq. (6): the evaporation gradient (the LHS term; black
800 bar), the coefficient gradient term (the first term on the RHS; yellow line), the wind
801 speed gradient term (the second term on the RHS; green line), the surface saturated
802 specific humidity term (the third term on the RHS; blue line), the air specific
803 humidity gradient term (the fourth term on the RHS; red line), and the residual term
804 (the last term on the RHS; gray line).

805

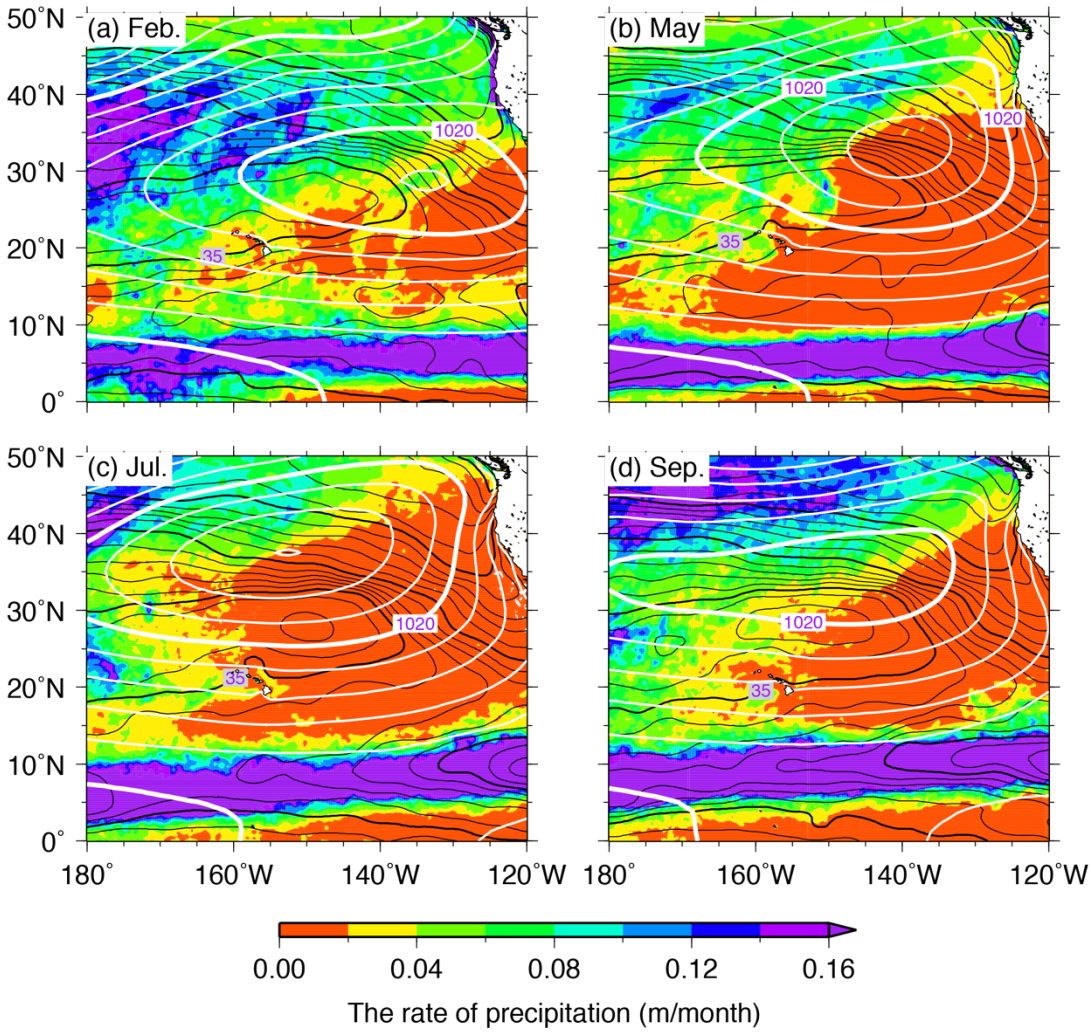

Fig. 11 As in Fig. 6, but for precipitation (color) in (a) February, (b) May, (c) July, and (d) September. Note that the precipitation gradient term [the second term on the RHS of Eq. (5)] has maximal values in May and September and minimal values in February and July.

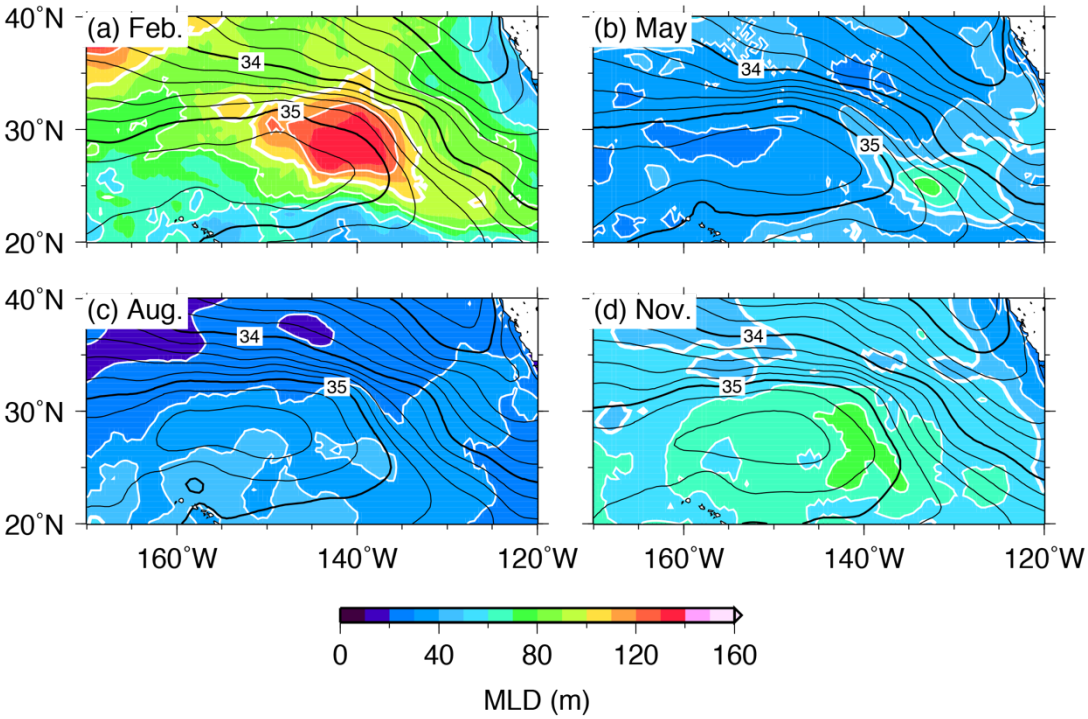

Fig. 12 As in Fig. 6, but for MLD (color and white contour). Thin (Thick) contour intervals are 20 (100) m in (a) and 10 (50) m in (b)–(d).

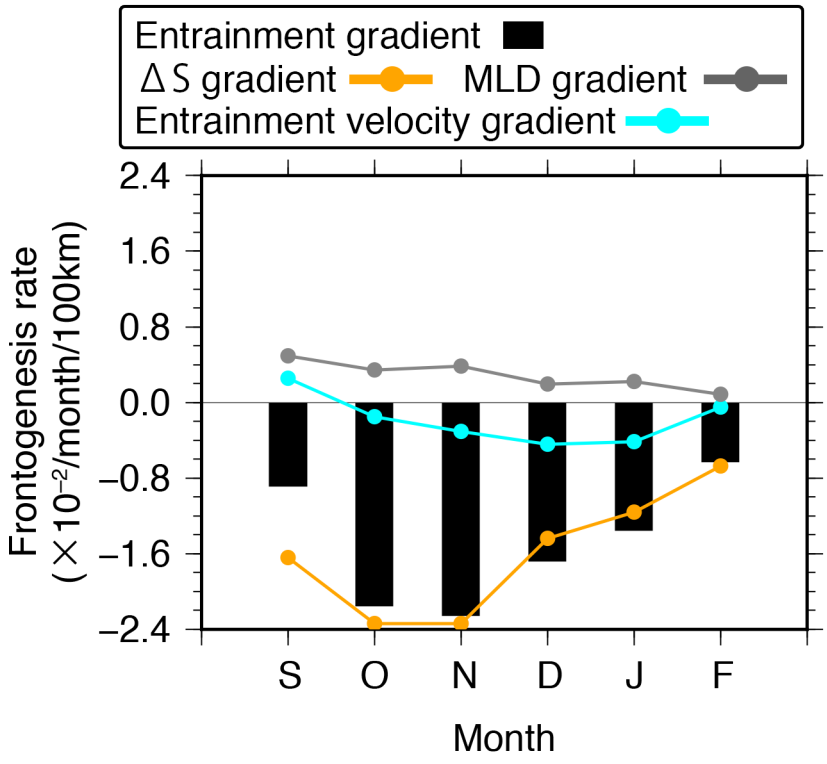

816

817 **Fig. 13** As in Fig. 4, but for Eq. (7) in September–February when the mixed layer
818 deepens on both sides of the front: the entrainment gradient term (the LHS term;
819 black bar), the salinity difference gradient term (the first term on the RHS; orange
820 line), the entrainment velocity gradient term (the second term on the RHS; cyan line),
821 and the MLD gradient term (the third term on the RHS; gray line).

822

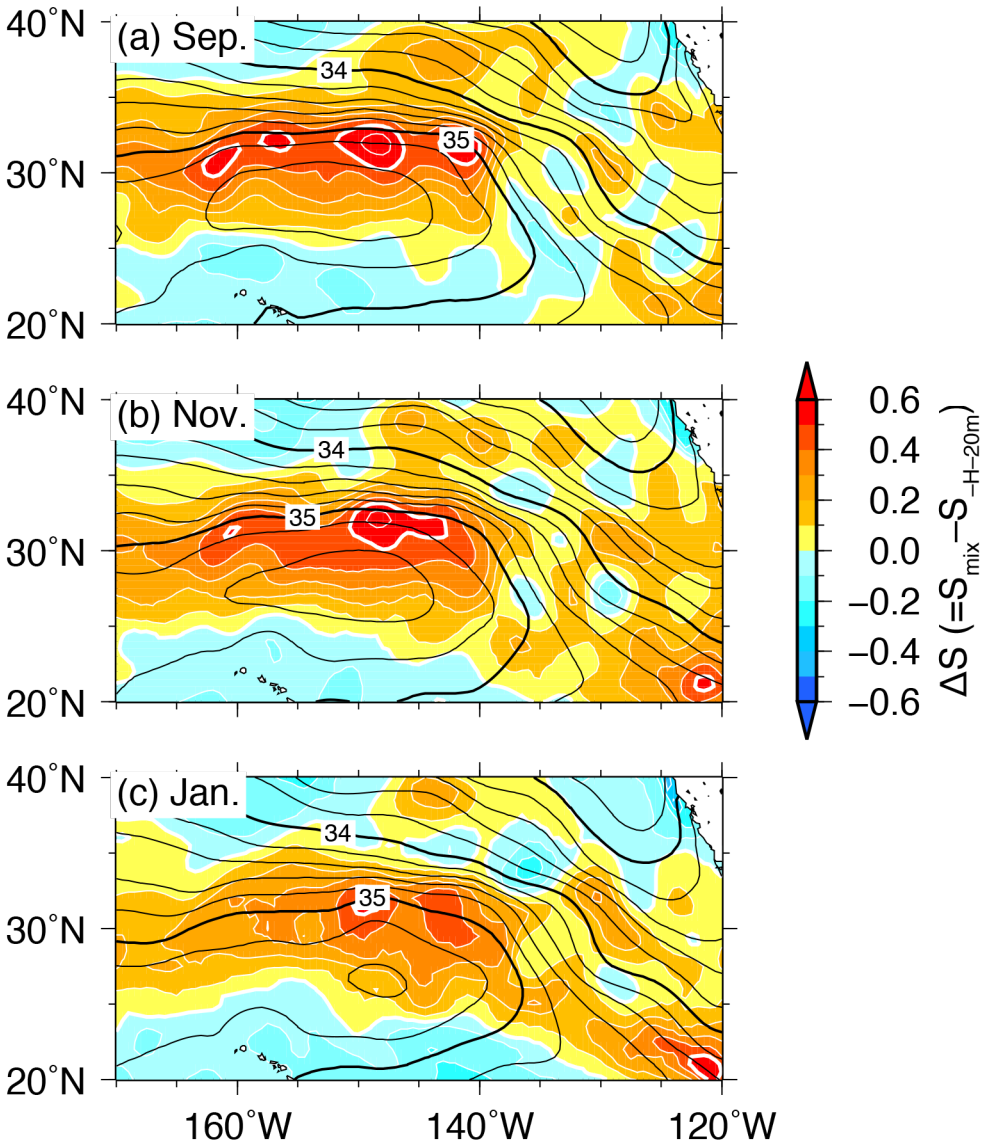

823

824 **Fig. 14** As in Fig. 6, but for the salinity difference between the mixed layer and

825 entrained water (color and white contour) in (a) September, (b) November, and (c)

826 January. Thin (Thick) white contour intervals are 0.1 (0.5).

827

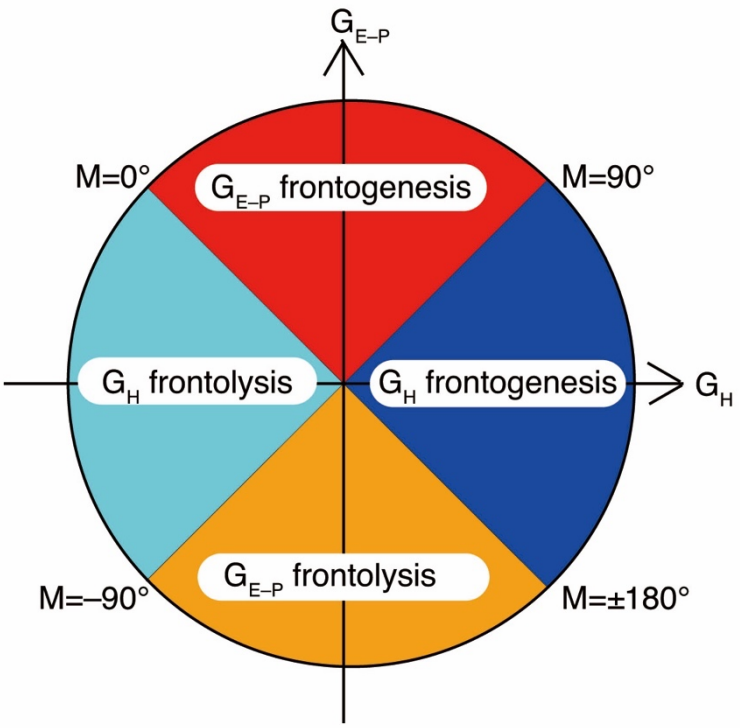

828

829 **Fig. 15** A schematic diagram to illustrate the definition and physical interpretation
830 of the freshwater flux frontogenesis metric M [Eq. (8)]. The horizontal MLS
831 gradient is strengthened by the horizontal gradients of freshwater fluxes and MLD
832 (G_{E-P} and G_H frontogenesis) when 0°<M<90° and 90°<M<180°, and relaxed by
833 those (G_{E-P} and G_H frontolysis) when –90°< M <0° and –180°< M <–90°,
834 respectively.

835

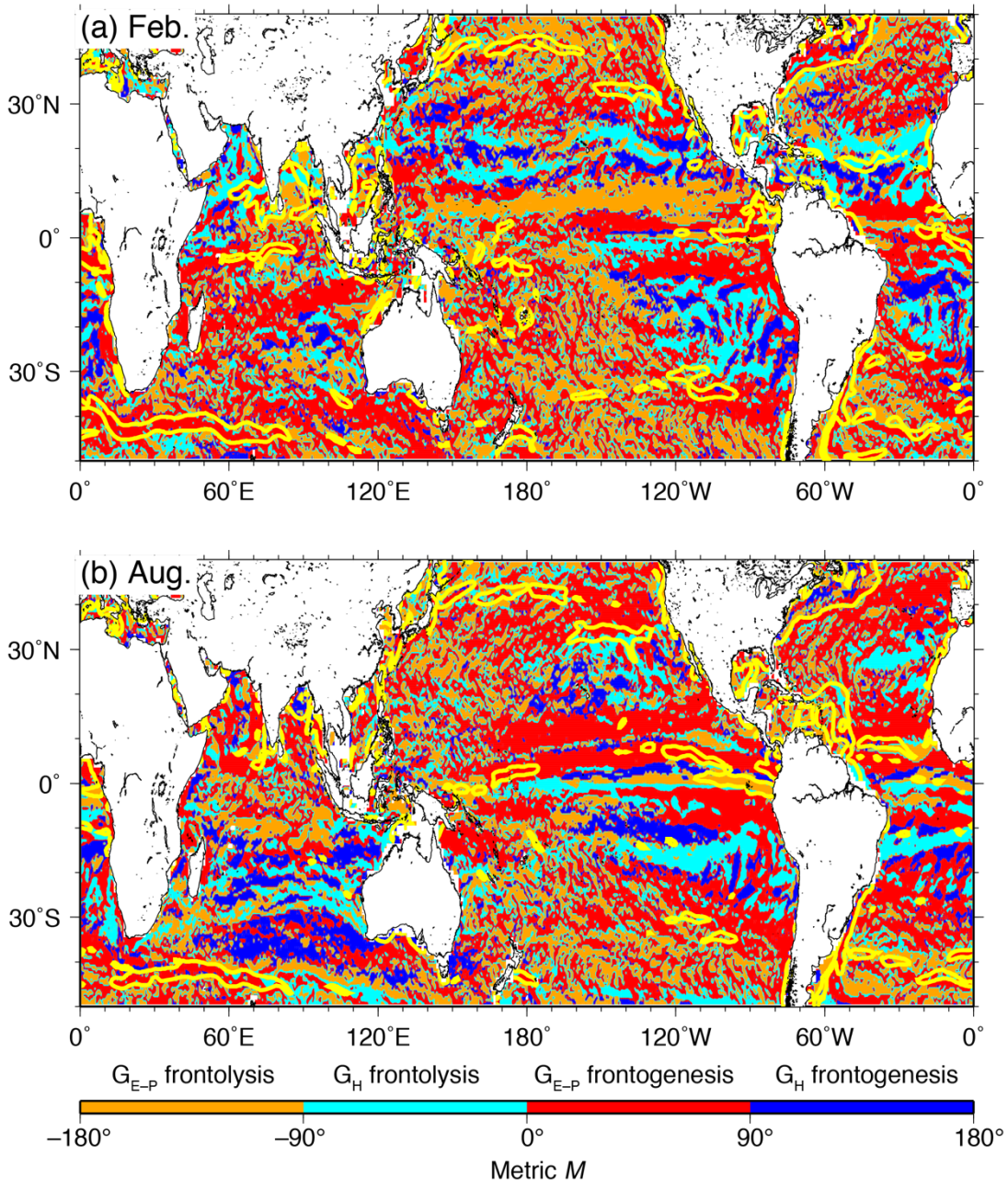

836

837 **Fig. 16** Global map of the freshwater flux frontogenesis metric in (a) February and

838 (b) August. Yellow lines enclose regions with the horizontal SSS gradient magnitude

839 larger than 0.2 $(100\text{km})^{-1}$.

840

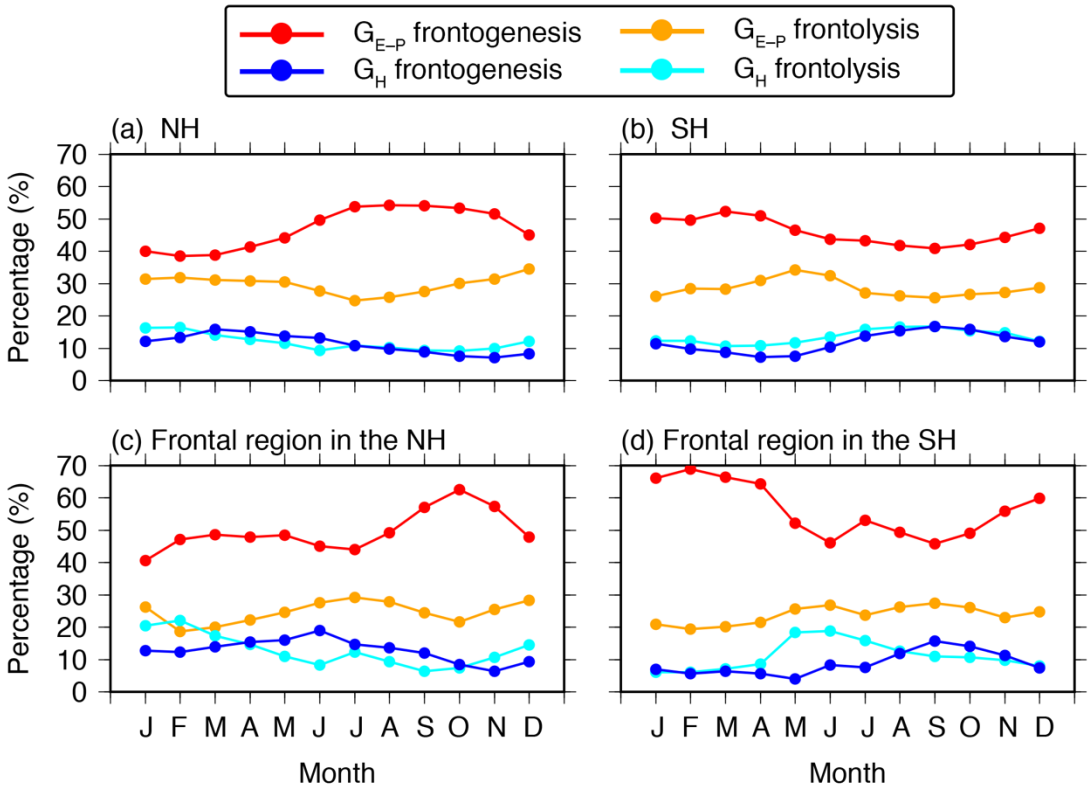

841

842 **Fig. 17** Monthly percentage of areas covered with each category of the freshwater

843 flux frontogenesis metric in the (a) Northern and (b) Southern Hemispheres. (c), (d)

844 As in (a), (b), but for frontal regions where the horizontal SSS gradient magnitude is

845 larger than 0.2 $(100\text{km})^{-1}$, respectively (see Fig. 16).

846

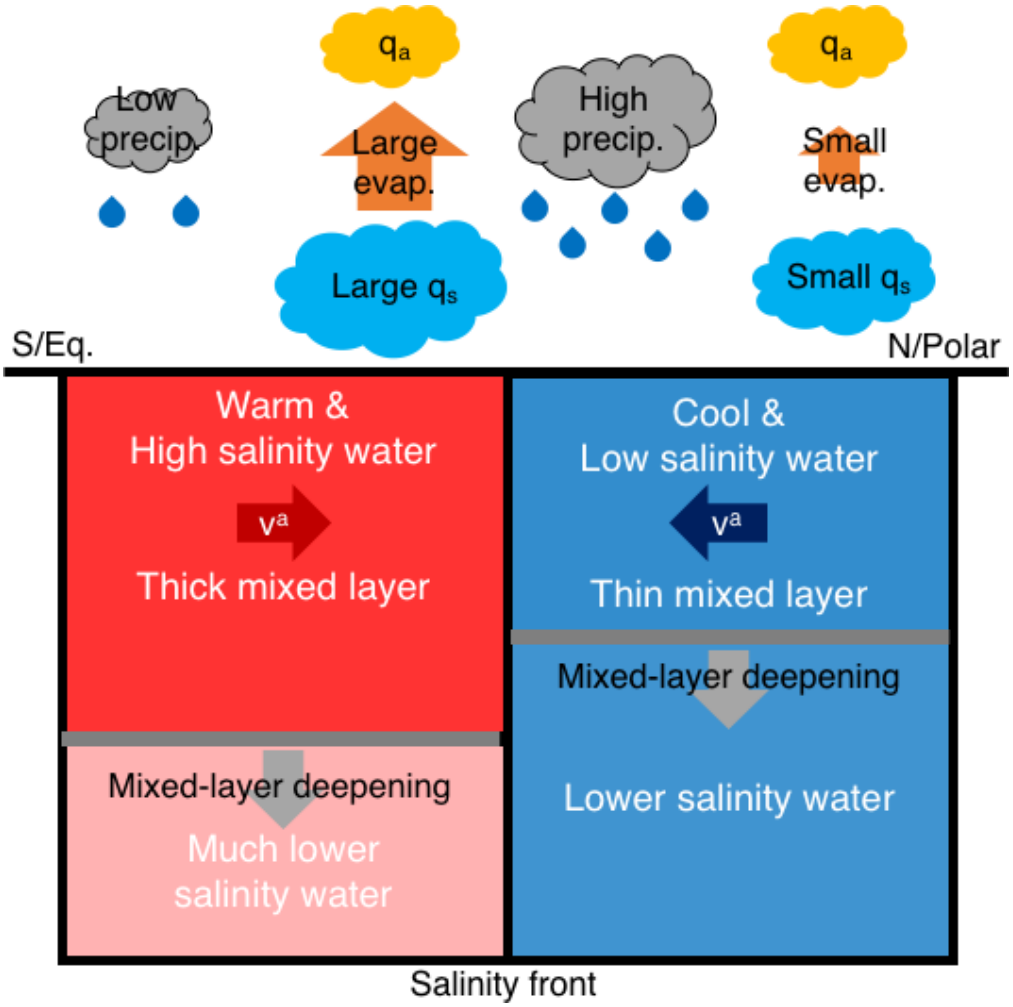

Fig. 18 A schematic diagram of salinity frontogenesis by freshwater fluxes and ageostrophic advection and frontolysis by entrainment during mixed-layer deepening phase (September–February) in the northeastern subtropical Pacific region. The upper red (blue) boxes represent mixed layers with high (low) salinity water separated by the mixed layer depth (gray line), the dark red (blue) arrows in the boxes indicate the meridional ageostrophic velocity. The light red (cyan) boxes below the mixed-layer boxes have much lower (lower) salinity water, and the gray vectors indicate mixed-layer deepening leading to the entrainment. Cyan (Orange) cloud-shape objects denote surface saturated (air) specific humidity, and orange vectors denote evaporation. Gray cloud-shape objects indicate the precipitation.

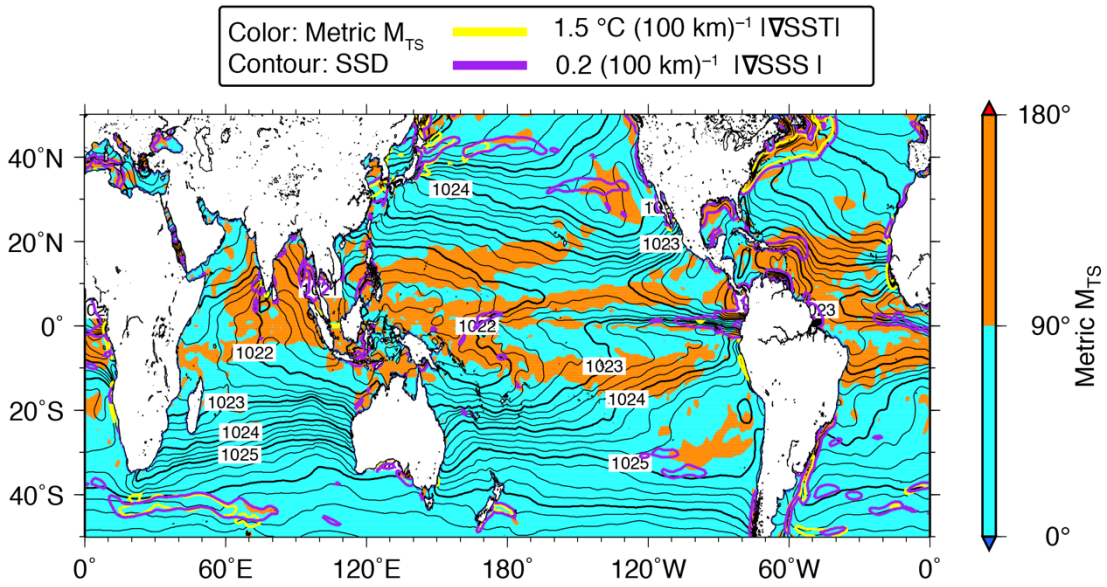

858

859 **Fig. A1** Global map of annual mean of sea surface density (SSD; contour) and a
860 metric M_{TS} [Eq. (A1); color] calculated from annual mean of SSTs, SSS, and SSD.
861 Yellow (Purple) contour lines enclose regions with the horizontal SST (SSS) gradient
862 magnitude larger than 1.5 °C (100 km)$^{-1}$ [0.2 (100 km)$^{-1}$]. Thin (Thick) contour
863 intervals are 0.25 (1) kg m^{-3}.

864

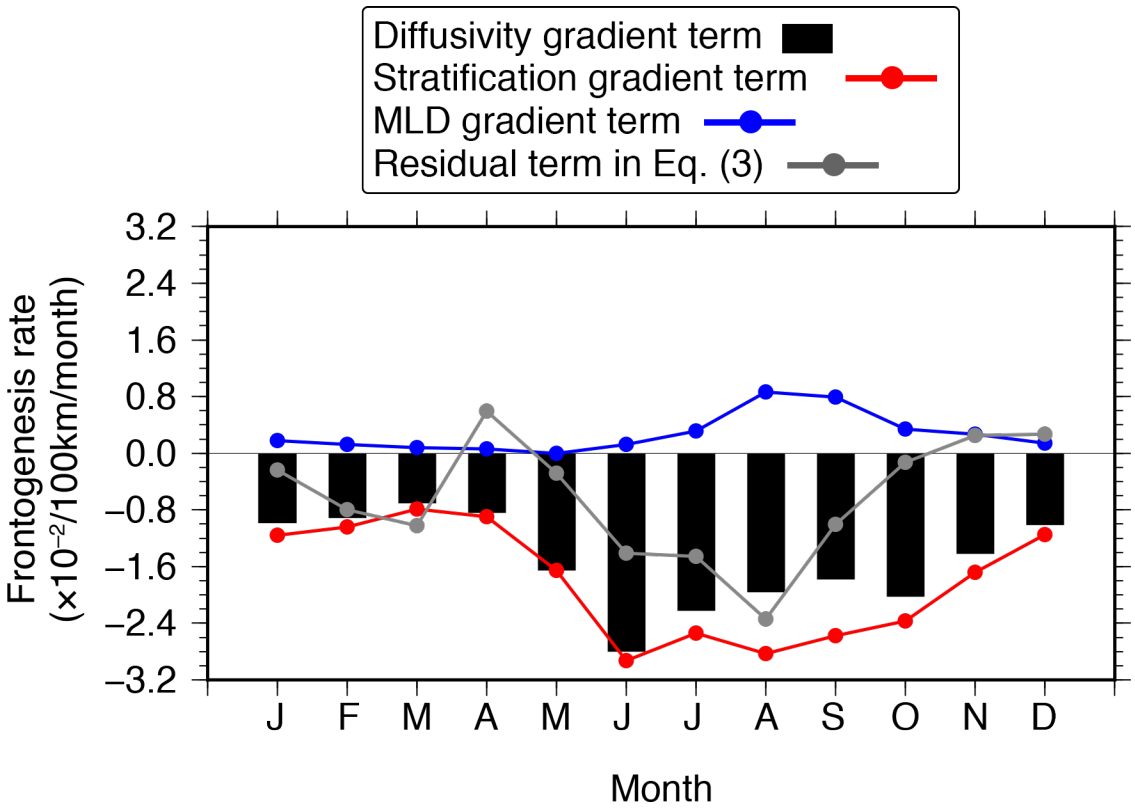

865

866 **Fig. A2** As in Fig.4, but for Eq. (A4): the vertical diffusivity gradient term (the LHS
867 term; black bar) and contributions from the salinity stratification (the first term on
868 the RHS; red line) and the MLD (the second term on the RHS; blue line). Gray line
869 denotes the residual term of the frontogenesis rate equation [the last term on the
870 RHS of Eq. (3)].

871